

**DETERMINATION OF BASALT PHYSICAL  
AND THERMAL PROPERTIES AT VARYING  
TEMPERATURES, PRESSURES, AND  
MOISTURE CONTENTS**

**Third Progress Report  
Fiscal Year 1979**

**August 31, 1979**

Prepared for Rockwell Hanford Operations,  
A Prime Contractor to the U. S. Department of Energy,  
Under Contract Number DE-AC06-77RL01030

**by:**

**Excavation Engineering and  
Earth Mechanics Institute**



**Colorado School of Mines  
Golden, Colorado**

## **DISCLAIMER**

**This report was prepared as an account of work sponsored by an agency of the United States Government. Neither the United States Government nor any agency Thereof, nor any of their employees, makes any warranty, express or implied, or assumes any legal liability or responsibility for the accuracy, completeness, or usefulness of any information, apparatus, product, or process disclosed, or represents that its use would not infringe privately owned rights. Reference herein to any specific commercial product, process, or service by trade name, trademark, manufacturer, or otherwise does not necessarily constitute or imply its endorsement, recommendation, or favoring by the United States Government or any agency thereof. The views and opinions of authors expressed herein do not necessarily state or reflect those of the United States Government or any agency thereof.**

## **DISCLAIMER**

**Portions of this document may be illegible in electronic image products. Images are produced from the best available original document.**

# N O T I C E

This report was prepared as an account of work sponsored by the United States Government. Neither the United States, nor the United States Department of Energy, nor any of their employees, nor any of their contractors, subcontractors, or their employees, makes any warranty, express or implied, or assumes any legal liability or responsibility for the accuracy, completeness, or usefulness of any information, apparatus, product or process disclosed, or represents that its use would not infringe privately owned rights.

DETERMINATION OF BASALT PHYSICAL  
AND THERMAL PROPERTIES AT VARYING  
TEMPERATURES, PRESSURES, AND MOISTURE CONTENTS

Third Progress Report  
Fiscal Year 1979

Russell J. Miller

August 31, 1979

DISCLAIMER

This book was prepared as an account of work sponsored by an agency of the United States Government. Neither the United States Government nor any agency thereof, nor any of their employees, makes any warranty, express or implied, or assumes any legal liability or responsibility for the accuracy, completeness, or usefulness of any information, apparatus, product, or process disclosed, or represents that its use would not infringe privately owned rights. Reference herein to any specific commercial product, process, or service by trade name, trademark, manufacturer, or otherwise, does not necessarily constitute or imply its endorsement, recommendation, or favoring by the United States Government or any agency thereof. The views and opinions of authors expressed herein do not necessarily state or reflect those of the United States Government or any agency thereof.

Prepared for Rockwell Hanford Operations,  
a Prime Contractor to U.S. Department of Energy,  
under Contract Number DE-AC06-77RL01030

N O T I C E

This report was prepared as an account of work sponsored by the United States Government. Neither the United States, nor the United States Department of Energy, nor any of their employees, nor any of their contractors, subcontractors, or their employees, makes any warranty, express or implied, or assumes any legal liability or responsibility for the accuracy, completeness, or usefulness of any information, apparatus, product or process disclosed, or represents that its use would not infringe privately owned rights.

EXCAVATION ENGINEERING AND  
EARTH MECHANICS INSTITUTE  
COLORADO SCHOOL OF MINES  
GOLDEN, COLORADO 80401

DISTRIBUTION OF THIS DOCUMENT IS UNLIMITED

TABLE OF CONTENTS

	Page
1.0 ABSTRACT	1
2.0 INTRODUCTION	2
3.0 TEST RESULTS	6
3.1 CHARACTERIZATION OF CORE SAMPLES	6
3.1.1 Procedures	6
3.1.2 Initial Sample Log	8
3.1.3 Initial Characterization	9
3.2 MEASUREMENT OF STRENGTH PROPERTIES OF INTACT CORE UNDER VARYING AMBIENT CONDITIONS	20
3.2.1 Apparatus	20
3.2.2 Test Specimens	20
3.2.3 Procedures	21
3.2.4 Calculation	22
3.2.5 Test Results	23
3.2.6 Test Data Analysis	23
3.3 MEASUREMENT OF STRENGTH PROPERTIES OF JOINTED CORE UNDER VARYING AMBIENT CONDITIONS	38
3.3.1 Apparatus	38
3.3.2 Test Specimens	38
3.3.3 Procedures	38
3.3.4 Calculation	39
3.3.5 Test Results	40
3.3.6 Test Data Analysis	40
3.4 MEASUREMENT OF THE THERMAL PROPERTIES OF INTACT CORE UNDER VARYING AMBIENT CONDITIONS	43
3.4.1 Thermal Conductivity/Specific Heat Procedures	43
3.4.1.1 Apparatus	43
3.4.1.2 Test Specimens	44
3.4.1.3 Procedures	44
3.4.1.4 Calculation	44
3.4.2 Thermal Expansion	46
3.4.2.1 Apparatus	46
3.4.2.2 Test Specimens	46
3.4.2.3 Procedures	46
3.4.2.4 Calculation	47
3.4.2.5 Test Results	47
3.4.2.6 Test Data Analysis	48

	Page
3.5 CREEP TESTS	49
3.5.1 Apparatus	49
3.5.2 Test Specimens	49
3.5.3 Procedures	49
3.5.4 Calculation	49
3.6 ROCK HARDNESS	50
3.6.1 Apparatus	50
3.6.2 Test Specimens	50
3.6.3 Procedures	50
3.6.4 Calculation	50
3.6.5 Test Results	50
3.6.6 Test Data Analysis	50
3.7 INVESTIGATION OF ANISOTROPY OF A SELECTED BASALT SAMPLE	53
3.7.1 Apparatus	53
3.7.2 Test Specimens	53
3.7.3 Procedures	53
3.7.4 Calculation	54
3.7.5 Test Results	54
3.7.6 Test Data Analysis	54
3.8 POST-FAILURE CHARACTERISTICS OF BASALT CORES	60
3.8.1 Apparatus	60
3.8.2 Test Specimens	60
3.8.3 Procedures	60
3.8.4 Calculation	60
3.8.5 Test Results	61
3.8.6 Test Data Analysis	61
3.9 PHYSICAL PROPERTIES	66
3.9.1 Apparatus	66
3.9.2 Test Specimens	66
3.9.3 Procedures	66
3.9.4 Calculation	66
3.9.5 Test Results	66
3.9.6 Test Data Analysis	67
4.0 GENERAL DISCUSSION	68
4.1 COMPARISON TO PREVIOUS RESULTS	68
4.2 LIMITATIONS OF SAMPLES, PROCEDURES, AND RESULTS	68
5.0 CONCLUSIONS	70
6.0 DISTRIBUTION	72

## LIST OF FIGURES

	Page
Figure 2.1 The Hanford Area	3
Figure 3.1 Failure Stress Versus Temperature	28
Figure 3.2 Young's Modulus Versus Temperature	30
Figure 3.3 Poisson's Ratio Versus Temperature	31
Figure 3.4 Failure Stress Versus Confining Pressure	33
Figure 3.5 Mohr's Envelope - Triaxial Results 3630' -3660'	34
Figure 3.6 Mohr's Envelope - Triaxial Results 3660' -3690'	35
Figure 3.7 Mohr's Envelope - Triaxial Results 3730' -3750'	36
Figure 3.8 Failure Stress Versus Strain Rate	37
Figure 3.9 Scleroscope Hardness Versus Depth of Core	52
Figure 3.10 P-Wave Velocity Versus Depth	59
Figure 3.11 Room Temperature Post-Failure Test Graph	62
Figure 3.12 Triaxially Confined Post-Failure Test Graph	63
Figure 3.13 High-Temperature Post-Failure Test Graph	64

## LIST OF TABLES

Table 3.1 Strength Properties of Intact Core as a Function of Confining Pressure	24
Table 3.2 Strength Properties of Intact Core as a Function of Temperature	25
Table 3.3 Strain Rates	26
Table 3.4 Inherent Joint Strengths and Slip Factors for Jointed Samples	41
Table 3.5 Thermal Expansion Coefficients	47
Table 3.6 Scleroscope Hardness Coefficients	51
Table 3.7 Dynamic Wave Velocities and Ratios in Axial and Radial Directions	55



Missing Page 1  
from  
Original Document

Missing Page 2  
from  
Original Document

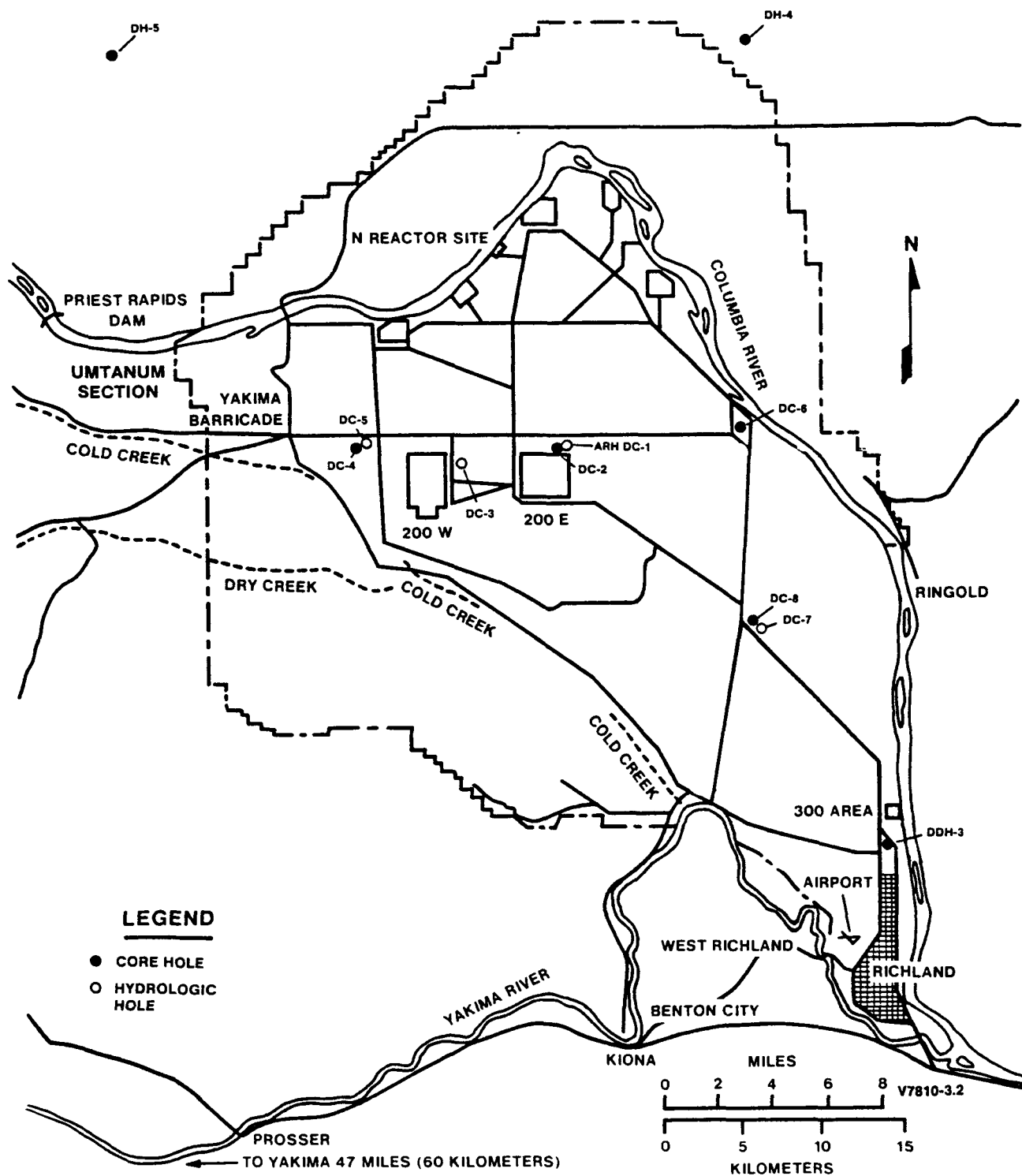


Figure 2.1: The Hanford Area

4. Thermal transport properties; i.e. conductivity and specific heat;
5. Thermal expansion;
6. Time-dependent deformation under various conditions of load and temperature;
7. Rock hardness;
8. Thermal or mechanical anisotropy;
9. Post-failure behavior;
10. Density.

It is necessary to know the strength properties of intact and jointed core for specifying opening geometry, pillar sizes, support requirements, and excavation methods. Young's modulus and Poisson's ratio are required for determining stress distributions and subsidence potential. Thermal properties are needed, as the canisters of waste material will heat the surrounding rock causing changes in stress, mechanical properties, and possibly long-term behavior of the repository. Time-dependent deformation, or creep, although expected to be minimal, could have an impact on subsidence, local fracturing, or the long-term stability of an opening. Rock hardness has implications in the areas of excavation methods and potential over break or blast damage into the walls of openings. If anisotropy exists, it is critical to any modeling effort to identify its prevalence and magnitude. Post-failure analysis identifies the remaining support capability of a pillar that, for some reason, may have failed. Failed pillars can still carry significant loads and can play an important part in support of a large areal underground opening. Density was determined for all samples, as a good correlation was previously found between density and many physical and thermal properties of basalt. And, as mentioned, the canisters of nuclear waste will heat the surrounding basalt, so it is important that the above properties be determined over the temperature range likely to be encountered.

Following is a presentation of the procedures, results, and discussion relevant to the physical and thermal properties discussed above.

### 3.0 TEST RESULTS

#### 3.1 CHARACTERIZATION OF CORE SAMPLES

##### 3.1.1 Procedures

The characterization of all core was accomplished through the following procedures:

1. Record date of receipt and sample designation of core, including locality, formation, drill hole number, and footage interval;
2. Photograph core in box as received using color Polaroid and Kodachrome film;
3. Rearrange in proper position any segments of core which have been jostled out of position in transit;
4. Spray core with water and wipe off drilling sludge for visual inspection;
5. Hand-lens description and identification of textural, structural, and mineralogical features of the core;
6. Binocular microscopic examination of features not readily discernible with hand lenses;
7. Preparation and microscopic petrographic analysis of selected thin sections of core to evaluate and amplify observations made megascopically and with the binocular microscope;
8. Integrate hand lens, binocular microscopic, and thin section microscopic data in final lithologic description of the core;
9. Close-up photography of selected segments of core to illustrate important lithologic features and variations;
10. Preparation of graphic log of core in 2 inch (in.) equals 1 foot (ft.) scale which describes in detail the fractures which are

present, as well as the mineralogy, texture fabric, and interflow features. Also, the location of all thin sections, test samples, and close-up photographs will be noted on the log.

In addition, to help define the effects of geologic structure upon basalt physical properties, those samples showing non-typical behavior and several representative samples were carefully characterized with respect to mineralogy and rock structure.

Based on the geologic characterization, areas within a line of core were identified for testing. The criterion for selecting an area for testing was that it represents a distinct group of geologic characteristics and that test specimens can be obtained from that area. In addition, a procedure was followed to assure, to the greatest extent possible, that the interrelated tests be performed on geologically similar samples. Thus, each group of tests is on samples from the same area of the core to maximize the validity of correlations between the various physical and thermal properties. Several of the tests are conducive to using the same sample and this was done when possible. Since variations in rock fabric, jointing, and mineralogy are likely to occur along the length of the core, each sample was described in detail and variations in physical or thermal behavior were correlated to the sample geologic characteristics.

Once a section of core was selected for testing, its dimensions were marked for cutting and a sample number, drill hole number, and a precise location were marked on it in indelible ink. It was at this point that the use of a core control sheet was initiated. On the sheet, the core was identified as to the test to be performed, sample number, drill hole, location, and core box number. The core was carefully described in terms of its geologic characteristics and then sent for preparation.

Following core preparation, the dimensions and quality of preparation were thoroughly checked before being sent for testing. For each test, there was a check-off procedure to assure correct test procedure and recording of data. Each test was observed and checked by the appropriate supervisor. Any calculations required were then performed and checked. If characteristics of the sample or procedure were believed to affect the results, this was noted on the control sheet. Finally, the data were collected and organized with a duplicate copy made and stored separately. Responsible individuals are required to sign off and each operation is monitored by a separate individual. A copy of the control sheet was maintained for each area of responsibility by the person in charge. This provides additional control and allows tracing and review of the testing procedure. In addition, numerous photographs were taken of the core at various stages providing a further control on sample identification.

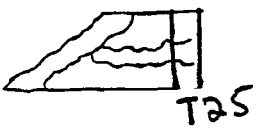
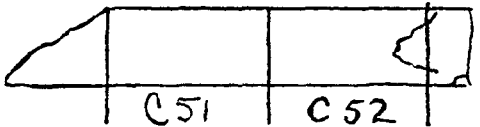
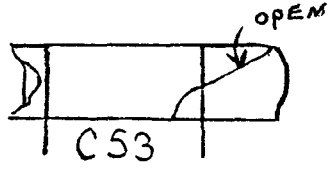
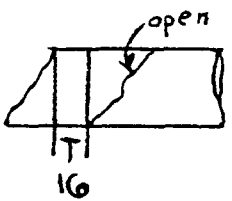
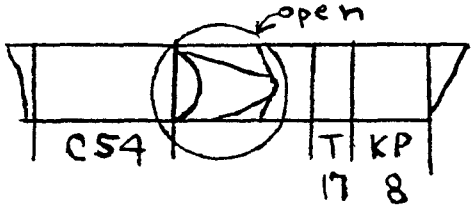
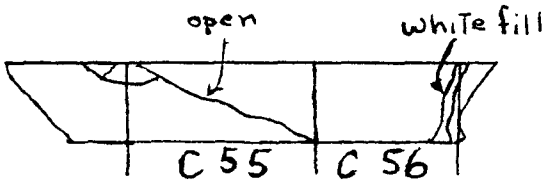
### 3.1.2 Initial Sample Log

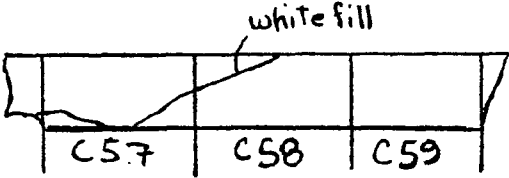

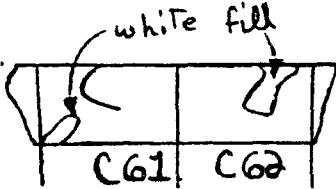
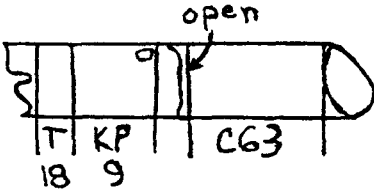
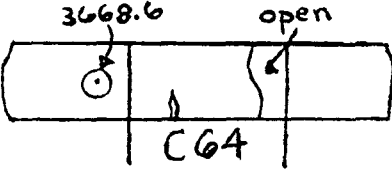
Following is the graphic log of the core as received, on a scale of 2 in. equals 1 ft. of core. Rockwell core box numbers, footages, and general descriptions of the cores are included, as well as the locations of the test samples. The sample designations are abbreviated as follows:

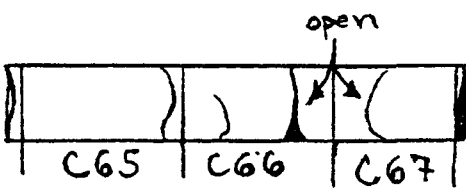
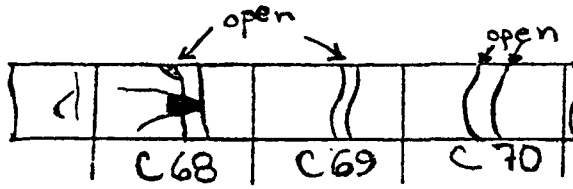
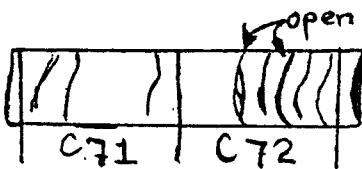
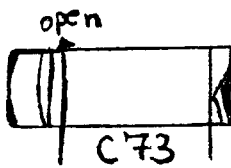
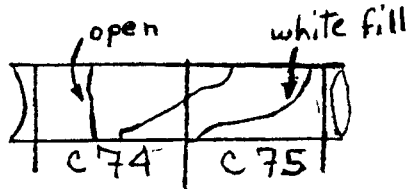
- U : uniaxial test specimen;
- TX : triaxial test specimen;
- TJ : jointed triaxial test specimen;
- PF : post-failure test specimen;
- UC : uniaxial creep test specimen;
- TS : thin section specimen;
- CP : specific heat test specimen;
- K : thermal conductivity test specimen;
- KP : thermal conductivity test specimen (recored perpendicular to core axis);
- XP : thermal expansion test specimen.

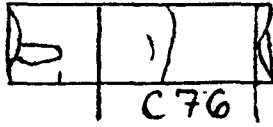


3.1.3 Initial Characterization

<u>Diagram</u>	<u>Footage</u>	<u>Description</u> (More detail in Lithologic Log following)
	3602.4- 3602.9	Porous
	3604.8- 3605.8	Porous
	3636.5- 3637.1	Porous
	3639.8- 3640.4	Porous
	3645.5- 3646.5	Porous, extremely cracked in middle
	3647.3- 3648.3	Slightly porous, white filling minor
	3649.2- 3650.2	Missing

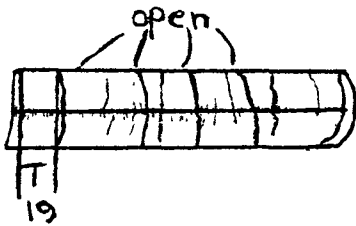
<u>Diagram</u>	<u>Footage</u>	<u>Description</u>
 <p>A horizontal rectangular diagram representing a core section. It is divided into three segments labeled C57, C58, and C59. A diagonal line from the top left corner of C57 to the bottom right corner of C58 is labeled 'white fill'.</p>	3655.5- 3656.6	White filling in joint
 <p>A horizontal rectangular diagram representing a core section. It is divided into two segments labeled C60 and T26. A small circle is drawn in the center of the T26 segment.</p>	3657.5- 3658.4	Solid basalt, small core missing
 <p>A horizontal rectangular diagram representing a core section. It is divided into two segments labeled C61 and C62. Both segments contain irregular, wavy lines representing joints. The area between these joints is labeled 'white fill'.</p>	3660.8- 3661.4	Minor jointing, white fill
 <p>A horizontal rectangular diagram representing a core section. It is divided into three segments labeled T18, KP9, and C63. The T18 and KP9 segments are further divided into sub-segments. A small circle is drawn in the C63 segment, and the area around it is labeled 'open'.</p>	3665.9- 3666.7	Minor white fill
 <p>A horizontal rectangular diagram representing a core section. It is divided into two segments labeled C64 and an unlabeled segment. A small circle is drawn in the C64 segment, and the area around it is labeled 'open'.</p>	3668.5- 3669.4	Solid basalt, one open joint

<u>Diagram</u>	<u>Footage</u>	<u>Description</u>
	3672.2- 3673.2	Slightly porous
	3673.2- 3674.6	Joints through each sample
	3675.7- 3676.5	Highly disced
	3682.5- 3683.1	Striated, disced
	3684.8- 3685.7	Dense basalt, critical joint angles

DiagramFootageDescription

3689.4-  
3690.0

Porous, intact



3695.5-  
3696.3

Highly striated and fractured



3699.7-  
3699.9

Small, striated segment



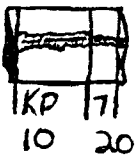
3703.1-  
3703.2

Too small to test



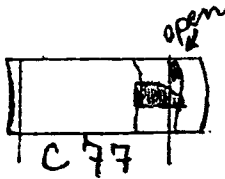

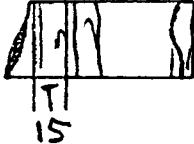
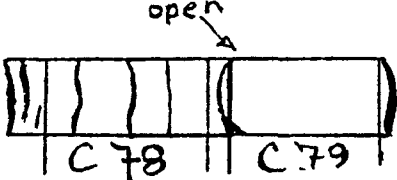
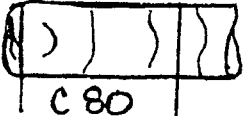
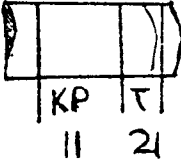
3704.4-  
3704.7

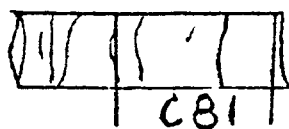
Solid basalt, joint parallel  
to core axis



3706.2-  
3706.5

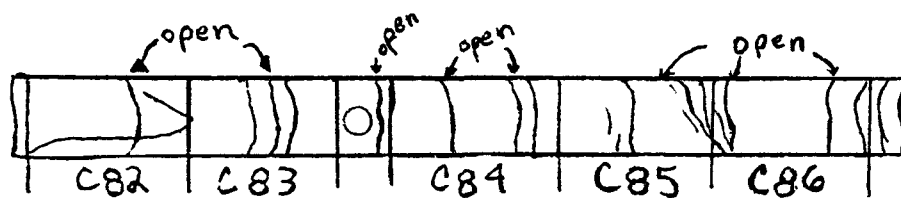
Central fractures parallel  
to core axis

<u>Diagram</u>	<u>Footage</u>	<u>Description</u>
	3710.2- 3710.8	Curvilinear joints, chips missing
	3725.5- 3725.7	Solid basalt
	3726.5- 3726.9	Striated
	3737.7- 3738.6	Solid basalt, horizontal striations
	3738.7- 3739.2	Dense, disced
	3739.3- 3739.7	Dense basalt

DiagramFootageDescription

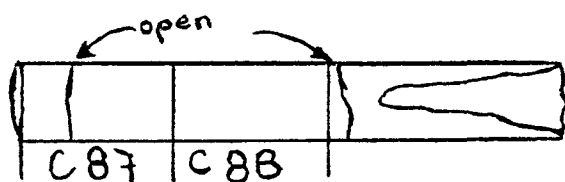
3747.8-  
3748.4

Striated



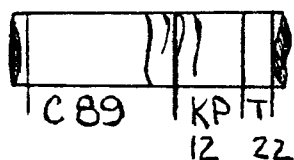
3754.6-  
3756.8

Open, layered striations  
throughout



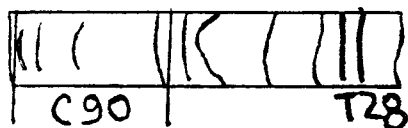
3756.8-  
3758.0

Solid basalt



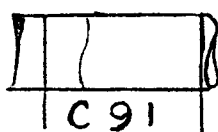
3765.0-  
3765.7

Fairly solid, striated



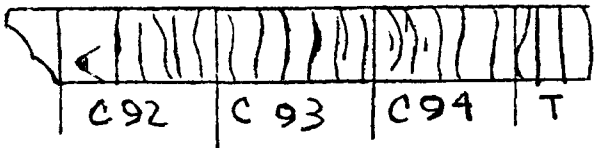
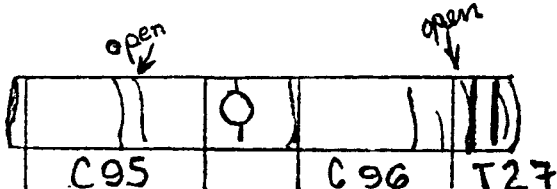
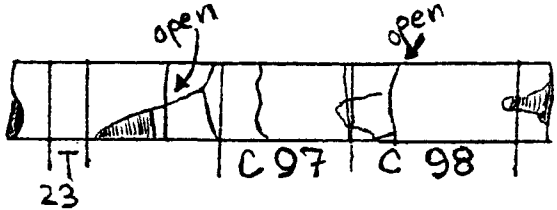
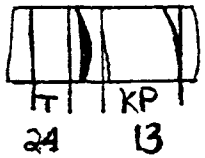

3767.6-  
3768.4

Parallel striation down core



3769.3-  
3769.7

Minor striations

<u>Diagram</u>	<u>Footage</u>	<u>Description</u>
	3782.5- 3783.9	Layered, frequent open striations throughout
	3785.6- 3786.7	Parallel striations
	3786.8- 3787.9	Open fractures, striations, chips missing
	3795.5- 3795.9	Parallel fractures, striations
	3810.2	Striated

## Series C - Lithologic Log

Drill Hole DC-4

Formation: Umtanum

<u>Box Nbr.</u>	<u>Footage</u>	<u>Description</u>
348 Flow Top	3602.4- 3602.9	Basalt; greenish-gray; microcrystalline; non-porphyrific with sparse microphenocrysts of plagioclase; vesicular, with vesicles up to 0.4 in. (1 cm.) elongate approximately perpendicular to core axis and probably parallel to flow layering; vesicles lined and partially filled with amygdules of chalcedony, quartz, waxy, very dark montmorillonite and zeolite(?); several irregular fractures at various angles to core axis; moderately microbrecciated and veined with secondary minerals listed above
348 Flow Top	3604.8- 3605.8	Lithology as above, with less microbrecciation and veining; irregular to curvilinear fractures coated with montmorillonite at 35-40° to core axis
352 Flow Top	3636.5- 3737.1	Lithology as above; some vesicles, cavities, and partial amygdules up to 1.4 in. (3.5 cm.); microbrecciated and veined as in interval 3602.4-3602.9
353 Flow Top	3639.8- 3640.4	Ditto
353 Flow Top	3645.5- 3646.5	Ditto; highly fractured, brecciated, and veined with secondary minerals at 3645.8-3646.2; some breccia fragments rotated from primary orientation in flow
353 Flow Top	3647.3- 3648.3	Primary lithology as above; some amygdules partially filled with silky, fibrous zeolite, probably natrolite or thomsonite; fractures at various angles to core axis
354 Flow Top	3649.2- 3650.2	Missing
354 Flow Top	3655.5- 3656.6	Lithology, structures, and secondary minerals as in 3602.4-3602.9, except considerably less vesicular and amygdaloidal; fractures and veins of secondary minerals up to 0.6 in. (1.5 cm.) wide at various angles to core axis
355 Central Flow	3657.5- 3658.4	Basalt; microcrystalline; non-porphyrific; dark gray to black; dense, hard; brittle; massive; occasional amygdale up to 0.6 in. (1.5 cm.) filled with silica minerals; tight, irregular fractures approximately equal to 20° to core axis; weak color banding approximately perpendicular to core axis probably represents flow layering



Drill Hole DC-4  
Formation: Umtanum

<u>Box Nbr.</u>	<u>Footage</u>	<u>Description</u>
355 Central Flow	3660.8- 3661.4	Ditto; 3660.9 amygdule 0.8 x 1.6 in. (2 x 4 cm.) filled with silica minerals laminated in depositional layers perpendicular to core axis; 3661.3 irregular amygdule 1.2 x 2.0 in. (3 x 5 cm.) filled with silica minerals; mottled flow laminations approximately perpendicular to core axis; few curvilinear fractures at various angles to core axis thinly coated with montmorillonite
356 Central Flow	3665.9- 3666.7	Ditto; vesicles and amygdules 0.04-2.6 in. (1 mm.-4 cm.)
356 Central Flow	3668.5- 3669.4	Ditto; less vesicular and amygdaloidal; less fractured
356 Central Flow	3672.2- 3673.2	Ditto; curvilinear fractures approximately perpendicular to core axis
357 Central Flow	3673.2- 3674.6	Ditto; somewhat darker in color; essentially black on freshly broken surface
357 Central Flow	3675.7- 3676.5	Ditto; curvilinear fractures spaced at approximately 0.6 in. (1.5 cm.) intervals approximately perpendicular to core axis and parallel flow layering; irregular, tightly cemented fractures approximately parallel to core axis
358 Central Flow	3682.5- 3683.6	Ditto; less fractured
358 Central Flow	3684.8- 3685.7	Ditto; several tight curvilinear fractures and veins of silica minerals and montmorillonite up to 0.08 in. (2 mm.) wide at 25° to core axis; lesser fractures approximately parallel to core axis
358 Central Flow	3689.4- 3690.0	As in interval 3675.7-3676.5
359 Central Flow	3695.5- 3696.3	Ditto
360 Central Flow	3699.7- 3699.9	Ditto

Drill Hole DC-4  
Formation: Umtanum

<u>Box</u> <u>Nbr.</u>	<u>Footage</u>	<u>Description</u>
360 Central Flow	3703.1- 3703.2	Ditto
360 Central Flow	3704.4- 3704.7	Ditto
360 Central Flow	3706.2- 3706.5	Ditto
361 Central Flow	3710.2- 3710.8	Ditto
362 Central Flow	3725.5- 3725.7	Ditto
362 Central Flow	3726.5- 3726.9	Ditto
363 Central Flow	3737.7- 3738.6	Ditto
363 Central Flow	3738.7- 3739.2	Ditto
364 Central Flow	3739.3- 3739.7	Ditto
364 Central Flow	3747.8- 3748.4	Ditto
365 Central Flow	3754.6- 3756.8	Ditto
366 Central Flow	3756.8- 3758.0	Ditto

Drill Hole DC-4  
Formation: Umtanum

<u>Box Nbr.</u>	<u>Footage</u>	<u>Description</u>
366 Central Flow	3765.0- 3765.7	Ditto
367 Central Flow	3767.6- 3768.4	Ditto
367 Central Flow	3769.3- 3769.7	Ditto
368 Central Flow	3782.5- 3783.9	Ditto; abundant light and dark gray flow laminations 0.04-0.20 in. (1-5 mm.) thick approximately perpendicular to core axis; numerous curvilinear fractures parallel flow lamination; few fractures 35-40° to core axis, thinly coated with montmorillonite
369 Central Flow	3785.6- 3786.7	As in interval 3769.3-3769.7, but with fewer fractures approximately perpendicular to core axis
369 Central Flow	3786.8- 3787.9	Ditto
369 Flow Bottom	3795.5- 3795.9	Ditto
370 Flow Bottom	3796.7- 3796.9	Missing

### 3.2 MEASUREMENT OF STRENGTH PROPERTIES OF INTACT CORE UNDER VARYING AMBIENT CONDITIONS

#### 3.2.1 Apparatus

The loading device used was a MTS Systems 1-million pound capacity "stiff" testing machine which is servo-controlled for loading rate or deformation rate control. In addition, the unit has the ability to interface directly with a PDP-11/05 computer for data analysis or testing program control.

For room-temperature testing, the confining pressure is applied to the specimen by a triaxial test chamber manufactured by Terrametrics, Inc. The hydraulic pressure to this cell is servo-controlled, assuring a constant level of confining pressure throughout the test.

Elevated-temperature triaxial testing is done in the Colorado School of Mines' Earth Mechanics Institute (EMI) custom-fabricated, high-temperature triaxial cell. This cell uses servo-controlled nitrogen pressure, with an internal 3 zone, 6 kilowatt resistance heater, which allows control of temperatures up to 500 degrees centigrade ( $^{\circ}\text{C}$ ).

Hardened steel platens were used conforming to American Society for Testing Materials (ASTM) requirements, as set forth in ASTM Standard D-2938. Spherical seats of the required size were employed for all tests.

#### 3.2.2 Test Specimens

Test specimens were right circular cylinders within tolerances specified in ASTM D-2938. The length was as close to two times the diameter as possible (except that shorter samples were required in the highly fractured sets of core tested under this contract). Exception was also taken to the ASTM D-2938 requirement for NX core (2-1/8 in. diameter), as most of the core was smaller in diameter (1-7/8 in.). The samples were oven dried overnight at  $90^{\circ}\text{C}$ , where

required. The diameter and length were determined to within 0.01 in. and the weight measured to 0.1 gram. For the tests at high temperatures, the samples were heated overnight at the desired temperature prior to testing.

### 3.2.3 Procedures

Before each series of tests, the calibration cylinder was loaded in the testing machine, and calibration and linearity checked. For a room-temperature triaxial test, the sample was centered in the membrane of the hydraulic triaxial cell, the lower platen was inserted at the bottom of the cell, and the upper platen at the top of the cell. The unit was then centered in the testing machine and the spherical seat placed on the upper platen. As a slight preload was applied to the sample, the spherical seat was adjusted to assure uniform seating. The desired confining pressure was then applied to the sample and a constant deformation rate was programmed into the testing machine to induce failure in approximately 10 minutes. At every 5 to 10 thousand pounds of incremental applied load, the load was held temporarily constant and strains recorded. The load-total deformation behavior was recorded on a chart recorder for a permanent record.

High-temperature triaxial tests were conducted similarly, but with additional equipment. The sample to be tested was placed in an aluminum can in a stainless steel sample holder, and heated in an oven to the desired (test) temperature. The sample in the holder was then loaded into the heating chamber of the high-temperature cell, the deflection probes positioned, outgas vent connected, and controller thermocouples placed. The cell was sealed, placed in the machine, preloaded, and the desired gas pressure selected on the pressure controller. A controlled deformation rate was programmed into the testing machine to induce failure in about 10 minutes. Again, the load,

radial deformation, and axial deformation behavior were recorded on a chart for a permanent record.

Uniaxial strain rate tests were conducted similarly, but much more simply due to the lack of elastic property measurements. If water-saturated, the sample was placed in the testing frame in a Ziploc plastic bag to keep the water from being driven off during the test. If heated, the sample was removed from the oven, wrapped in a flexible ceramic insulation sheath, and placed in the test frame. A spherical seat was lubricated and centered atop the sample, and a variable deformation rate (calculated to be from 1000 to 100,000 microstrains in the sample per minute) was programmed into the machine, and the sample loaded to failure. For samples heated to 300-500°C, the spherical seat was also heated in the oven to minimize sample heat losses. The load-total deformation behavior was recorded via chart recorder and included with the final report.

#### 3.2.4 Calculation

The compressive strength of the sample was calculated by dividing the maximum load carried by the sample by the cross-sectional area of the sample. Where samples shorter than 2 times the diameter had to be tested, their compressive strength was adjusted for a 2:1 specimen by using the equation:

$$C = C_a / 0.88 + 0.24 (b/h) \quad (1)$$

where

C = computed compressive strength of an equivalent L/D = 2 specimen (ksi);

C<sub>a</sub> = measured compressive strength of the specimen tested (ksi);

b = test core diameter (in);

h = test core height (in).

### 3.2.5 Test Results

Three sets of strength tests were done on the intact cores: triaxial, while varying confining pressure; triaxial, while varying sample temperature; and uniaxial, while varying sample temperature, water saturation, and strain rate. Triaxial tests with varying confining pressure were conducted at room temperature, with 3 repetitions each at 50 pounds per square inch gauge pressure (psig) with fresh samples, 50 psig with samples heated to 500°C and cooled, 2500, 5000, and 7500 psig. Triaxial tests at varying sample temperatures were conducted at 50 psig nitrogen pressure, with 3 repetitions each at 20°C water-saturated, 20°C oven-dried, 150, 300, and 500°C. Uniaxial tests were conducted at 4 strain rates: 1000, 10,000, 25,000, and 100,000 micro-strains per minute; at 5 temperature conditions each: 20°C water-saturated; 20°C oven-dried, 150, 300, and 500°C.

Table 3.1 presents the results obtained on the varying confining pressure triaxial tests. Table 3.2 presents the results obtained by varying temperature. Table 3.3 shows the results obtained by the uniaxial strain rate tests. In all cases, the results are presented in order of increasing depth.

### 3.2.6 Test Data Analysis

As in the two earlier series of tests, the upper portions of the flow showed significantly lower values of strength and Young's modulus than the central and lower portions of the flow. The upper portion of the flow was generally characterized by various degrees of vesiculation, alteration, and clastic appearance. Similar changes in color and texture occurred, as were noted for those in Series A (drill hole DC-6) and Series B (drill hole DC-8).

An effect of temperature on strength might be deduced from the data for this series of tests, as shown in Figure 3.1. There appears to be a steady decrease of average strength with increasing temperature, but the standard deviations remain large. Although not conclusive, the earlier results of

TABLE 3.1

## STRENGTH PROPERTIES OF INTACT CORE AS A FUNCTION OF CONFINING PRESSURE

<u>Depth (ft)</u>	<u>Sample Number</u>	<u>Density (gm/cc)</u>	<u>Test Conditions</u>	<u>Failure Stress (ksi)</u>	<u>Young's Modulus (10<sup>6</sup>psi)</u>	<u>Poisson's Ratio</u>
3605.2	C151	2.42	hot/cool	16.68	5.39	0.440
3636.7	C153	2.33	0 psi	4.71	3.05	0.448
3645.7	C54	2.62	2500 psi	40.40	18.86	0.497
3656.3	C159	2.64	7500 psi	65.14	8.11	0.160
3657.6	C60	2.66	5000 psi	60.35	8.20	0.170
3660.9	C161	2.65	hot/cool	25.56	7.32	0.262
3668.9	C64	2.77	0 psi	40.63	9.10	0.189
3672.7	C166	2.70	5000 psi	52.13	4.44	0.138
3682.8	C73	2.76	5000 psi	72.50	14.20	0.903
3738.3	C79	2.78	7500 psi	83.40	-	-
3738.3	C179	2.78	7500 psi	25.51	14.54	0.512
3738.8	C180	2.77	0 psi	28.77	16.95	0.524
3748.1	C181	2.80	2500 psi	38.57	2.93	0.098
MEAN VALUES AND		2.62	0 psi	24.71	9.70	0.387
		$\pm 0.25$		$\pm 18.30$	$\pm 6.97$	0.175
STANDARD DEVIATION		2.54	hot/cool	21.12	6.36	0.351
AT EACH		$\pm 0.16$		$\pm 6.28$	$\pm 1.36$	0.126
PRESSURE		2.71	2500 psi	39.49	10.90	0.298
		$\pm 0.13$		$\pm 1.29$	$\pm 11.26$	0.282
		2.71	5000 psi	61.66	8.95	0.404
		$\pm 0.05$		$\pm 10.25$	$\pm 4.92$	0.433
		2.73	7500 psi	58.02	11.33	0.336
		$\pm 0.08$		$\pm 29.59$	$\pm 4.55$	0.249



TABLE 3.2

STRENGTH PROPERTIES OF INTACT CORE AS A FUNCTION OF TEMPERATURE

Depth (ft)	Sample Number	Density (gm/cc)	Temperature (°C)	Failure Stress (ksi)	Young's Modulus (10 <sup>6</sup> psi)	Poisson's Ratio
3647.7	C155	2.67	500	16.19	2.45	0.238
3656.3	C59	2.65	20	22.09	10.13	0.272
3660.9	C61	2.64	500	11.04	0.69	0.258
3672.4	C65	2.76	150	30.73	5.16	1.560
3674.2	C70	2.73	20 wet	24.41	7.28	0.133
3674.3	C170	2.74	20	28.11	9.41	0.733
3676.2	C72	2.76	150	28.46	6.18	0.419
3682.8	C173	2.78	300	23.77	1.55	0.136
3738.8	C80	2.78	20 wet	4.98	10.44	0.200
3754.7	C82	2.82	300	34.30	6.45	0.279
3756.9	C187	2.82	20	26.48	14.79	0.286
3783.4	C94	2.78	300	22.17	3.23	0.121
3785.7	C195	2.78	500	18.11	3.00	0.859
3786.3	C196	2.75	20 wet	13.07	5.10	0.335
MEAN VALUES		2.74	20 dry	25.56	11.44	0.430
STANDARD DEVIATIONS AT EACH		+0.09		+ 3.11	+ 2.92	+ .262
TEMPERATURE		2.75	20 wet	14.15	7.61	0.223
		+0.03		+ 9.76	+ 2.68	+ .103
		2.76	150	29.60	5.67	0.990
		+0.00		+ 1.61	+ 0.72	+ .807
		2.79	300	26.75	3.75	0.179
		+0.02		+ 6.59	+ 2.49	+ .087
		2.70	500	15.11	2.05	0.452
		+0.07		+ 3.66	+ 1.21	+ .352

TABLE 3.3

## STRAIN RATES

Depth (ft)	Sample Number	Density (gm/cc)	Temperature (°C)	Strain Rate ( $\mu\epsilon/\text{min}$ )	Failure Stress (ksi)
3605.3	C51	2.37	20 saturated	1000	6.02
3636.7	C53	2.48	150	10000	11.48
3645.7	C154	2.64	500	25000	12.06
3647.7	C55	2.62	300	1000	12.33
3655.7	C57	2.65	150	100000	15.83
3657.6	C160	2.72	500	10000	18.59
3666.5	C63	2.73	20	10000	29.48
3666.5	C163	2.75	20 saturated	25000	24.28
3673.9	C169	2.74	300	10000	13.84
3675.8	C71	2.71	150	25000	12.40
3676.2	C172	2.77	20	1000	31.02
3710.3	C77	2.76	300	100000	22.69
3748.1	C81	2.76	20	25000	42.63
3755.0	C83	2.77	500	100000	5.01
3755.0	C183	2.77	150	1000	33.37
3757.2	C188	2.81	20 saturated	10000	11.50
3765.1	C189	2.77	300	25000	12.49
3769.5	C91	2.8	500	1000	6.44
3785.7	C95	2.72	20	100000	46.67
3787.4	C97	2.77	20 saturated	100000	11.20
MEAN VALUES AND		2.74	20 dry		37.45
STANDARD DEVIATION		$\pm 0.02$			$\pm 8.50$
TIONS AT EACH		2.67	20 wet		13.32
TEMPERATURE		$\pm 0.20$			$\pm 7.75$
		2.65	150		18.27
		$\pm 0.12$			$\pm 10.24$
		2.72	300		15.33
		$\pm 0.07$			$\pm 4.95$
		2.73	500		10.52
		$\pm 0.07$			$\pm 6.18$

Table 3.3 Continued

	Density (gm/cc)	Strain Rate ( $\mu\epsilon/\text{min}$ )	Failure Stress (ksi)
MEAN VALUES AND	2.67	1000	17.84
STANDARD DEVIATIONS AT EACH	$\pm 0.18$		$\pm 13.37$
	2.70	10000	16.91
	$\pm 0.13$		$\pm 7.61$
STRAIN RATE	2.73	25000	20.77
	$\pm 0.05$		$\pm 13.27$
	2.73	100000	20.28
	$\pm 0.05$		$\pm 16.11$

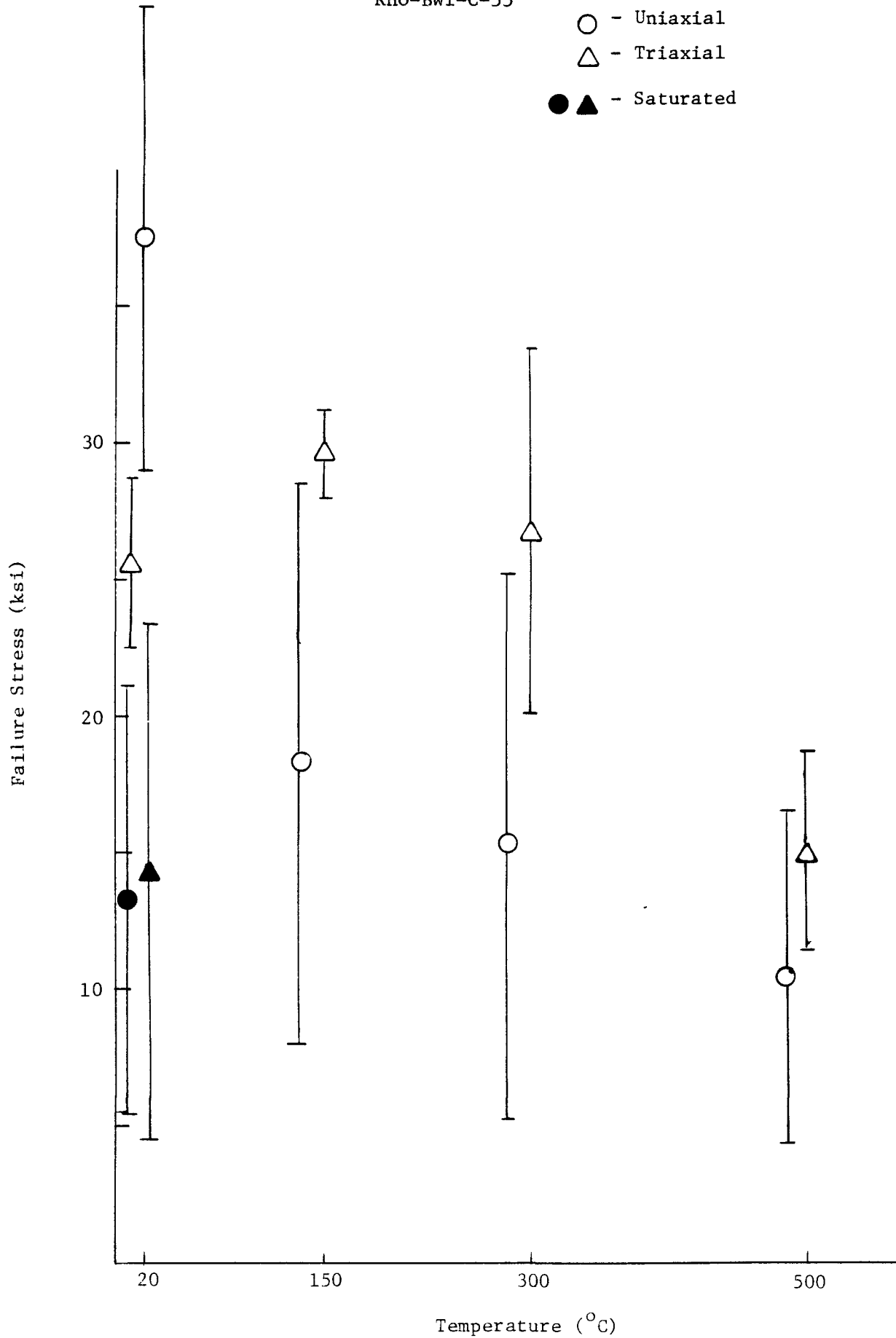


Figure 3.1: Failure Stress Versus Temperature

Series A and Series B did indicate that strengths may diminish at higher temperatures. Considering the three series of tests, it is possible to conclude a temperature effect on strength, but the effect is probably within expected strength variations without considering temperature. The saturated samples showed strengths significantly below those determined for dry samples at room temperature. These results agree with the results of Series B, but opposite to the trend exhibited in Series A. Observations noted in preparing and testing creep samples were that the saturated samples could not maintain the creep loads imposed, nor could the non-saturated samples. Since failure generally occurred along joint surfaces, it would appear that exposure to water deteriorates the joint infilling material, thus reducing strength. Since the core was at one time exposed to moisture (i.e., drilling mud), it would appear that the reduction of strength resulting from saturation is reversible upon drying of the core.

Again, as in Series A and Series B, the average strength for the heated and cooled samples was lower than the dried samples, but the small difference and large standard deviations make it difficult to conclude an effect of temperature cycling for this series of tests.

Young's modulus, as shown in Figure 3.2, showed a similar reduction with increasing temperature, as was observed for compressive strength. The magnitude of the reduction was unexpected, as no such dramatic effects of temperature on modulus were observed in the previous two series of tests.

Poisson's ratio results showed considerable scatter with some excessively high values, possibly due to localized surface effects. As can be seen in Figure 3.3, it would be difficult to conclude the effect of temperature on Poisson's ratio.

Moisture content, heating, and cooling appear to have an indeterminate effect on Young's modulus and Poisson's ratio.

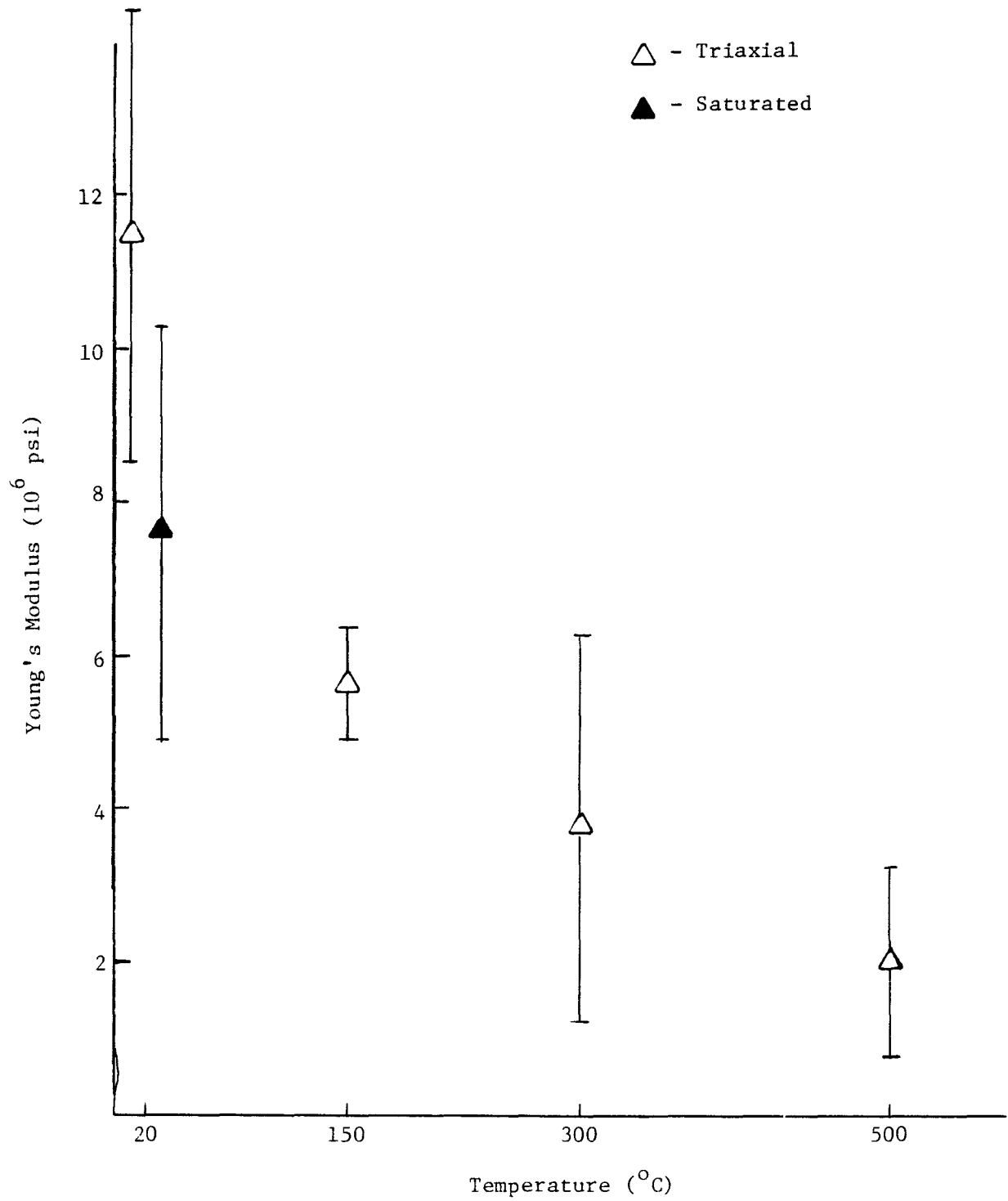


Figure 3.2: Young's Modulus Versus Temperature

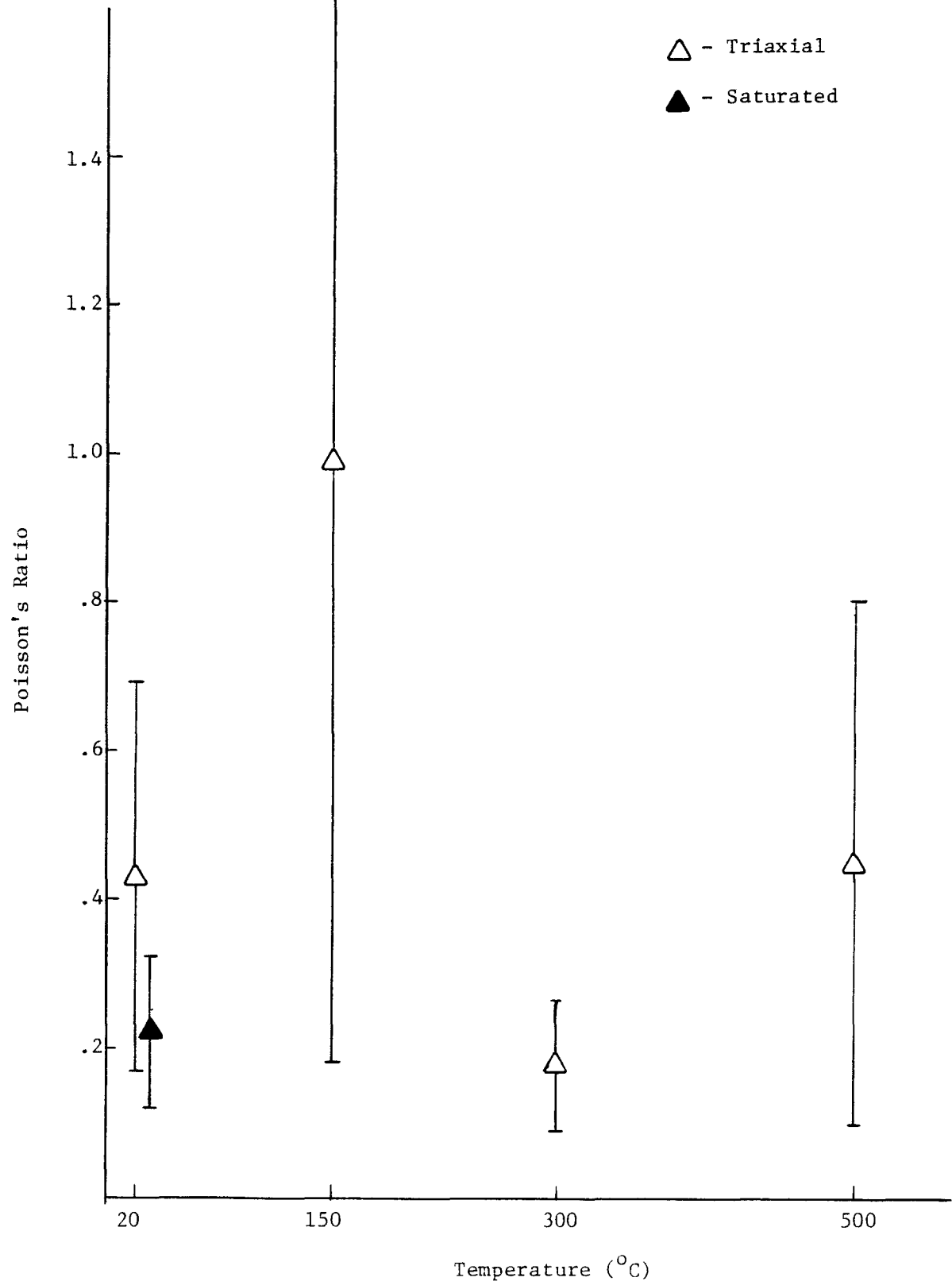


Figure 3.3: Poisson's Ratio Versus Temperature

The effect of confining pressure on the compressive strength of basalt from drill hole DC-4 is evidenced in Figure 3.4. A nearly three-fold increase in strength occurs between ambient and 10,000 psi confining pressure. As in Series B, the beneficial effect of confining pressure is evidenced by the average of all confined compressive strengths being more than twice the average for the unconfined compressive strengths.

Mohr envelope analyses were performed over three depth ranges, and are shown in Figures 3.5, 3.6, and 3.7. Friction angles were fairly consistent in the range of  $41-52^{\circ}$ . This compares with a friction angle determined for Series A of  $36-44^{\circ}$ , and for Series B of  $45-50^{\circ}$ .

Failure stress versus strain rate for the Series C cores is presented in Figure 3.8. A slight increase in strength with increased strain rate was observed; but, with the large standard deviations obtained, a definite conclusion as to the effect of strain rate could not be derived.

Comparing the results of the Series C compressive strength tests with those of Series A and Series B, average strengths were comparable between Series A and Series C; however, Series B appears to have had significantly lower strength than both Series A and Series C. As similar observations can be made for Young's modulus as for strength, it would appear that intact core from Series A (drill hole DC-6) and Series C (drill hole DC-4) have similar physical properties and also correlate fairly well with FY 78 results. Series B (drill hole DC-8), however, appears to vary from the other core locations.



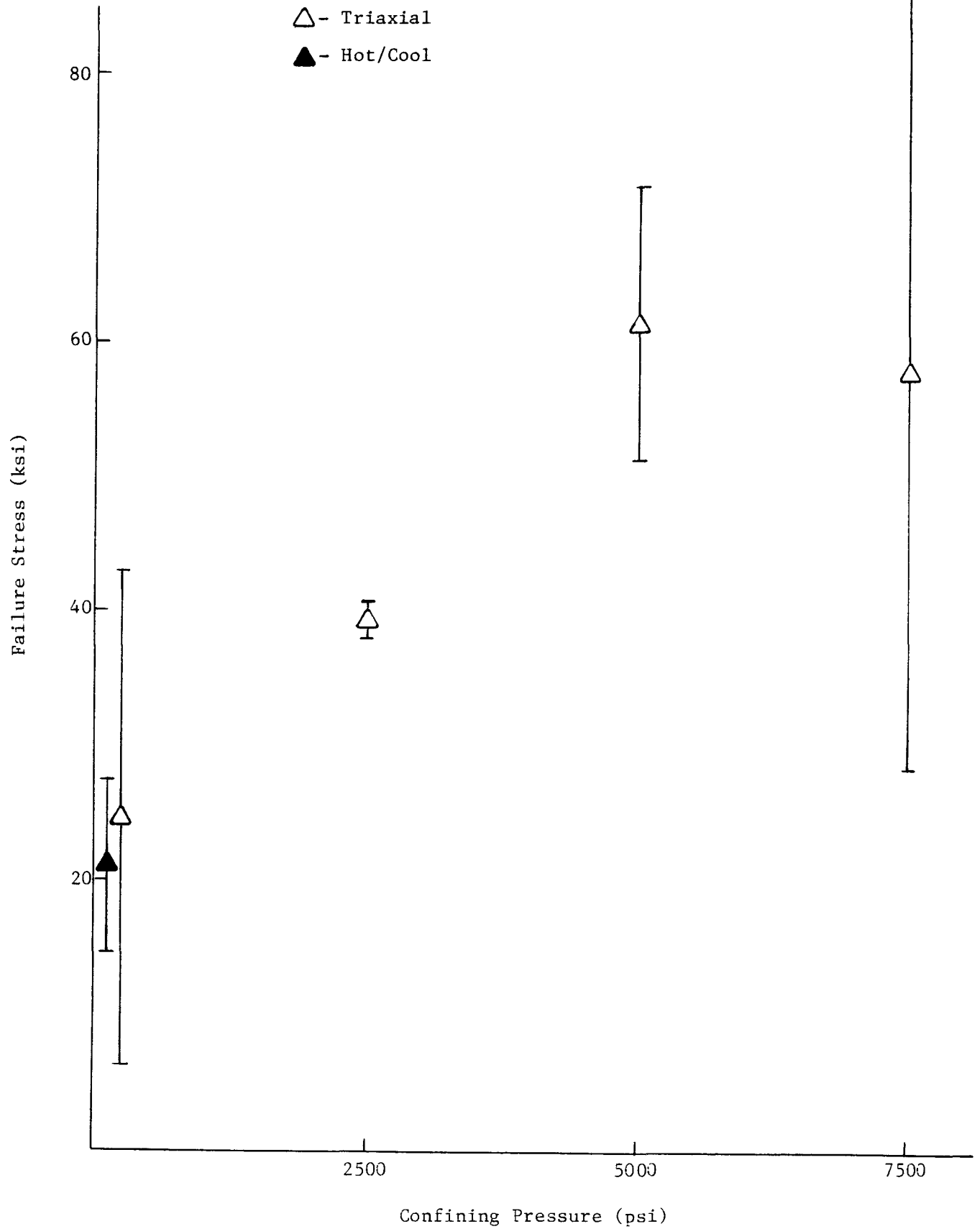


Figure 3.4: Failure Stress Versus Confining Pressure

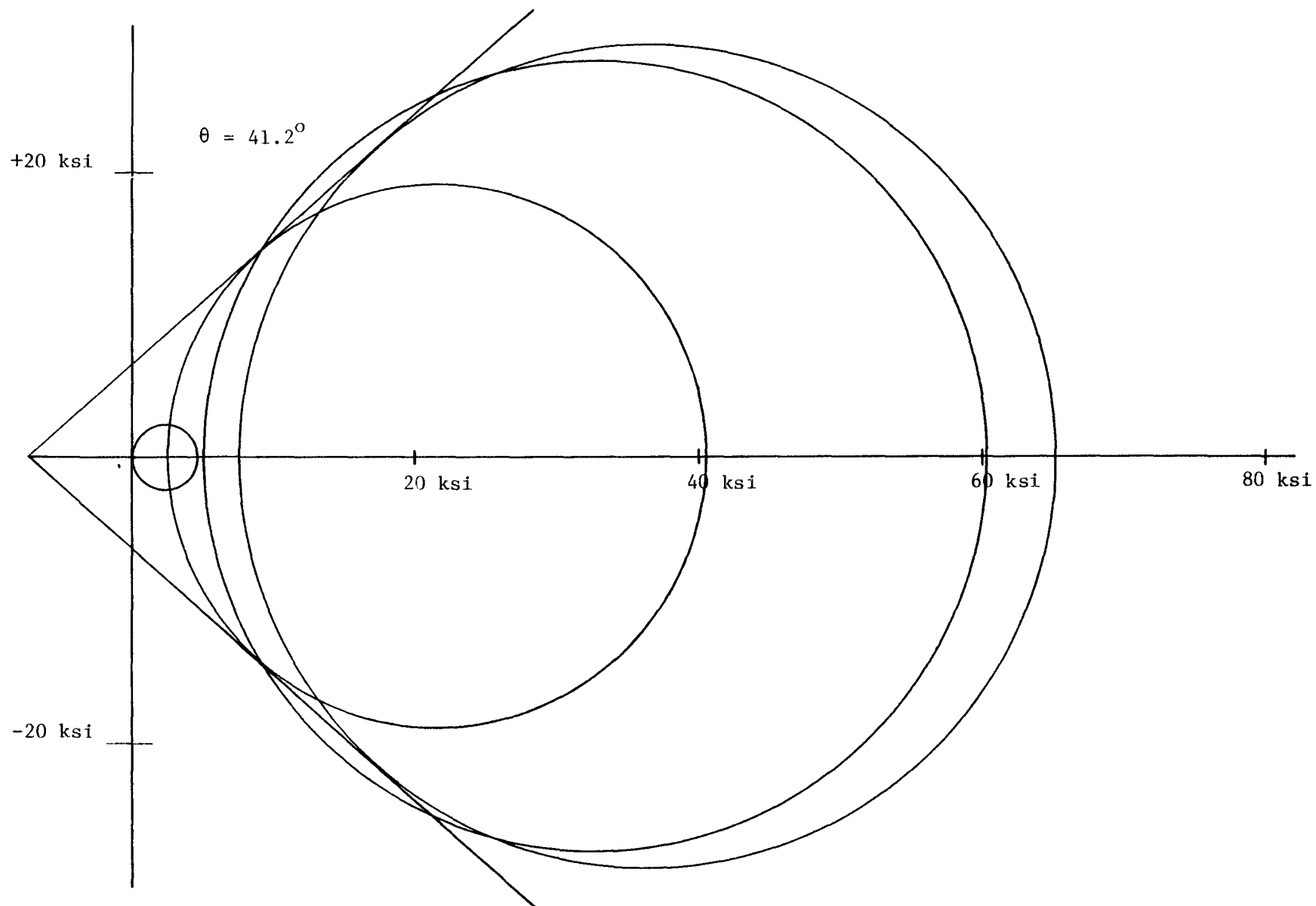


Figure 3.5: Mohr's Envelope - Triaxial Results 3630'-3660'

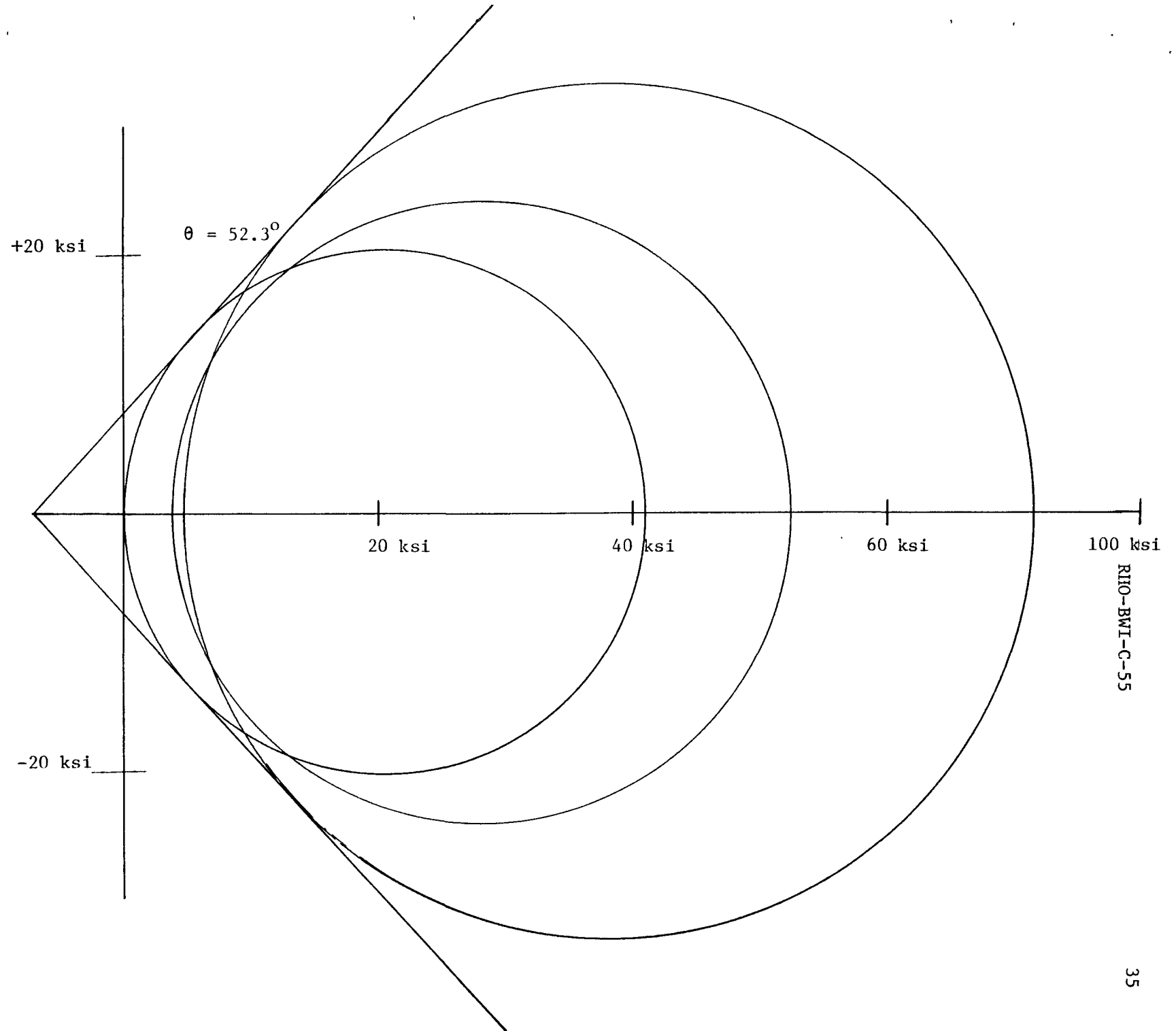
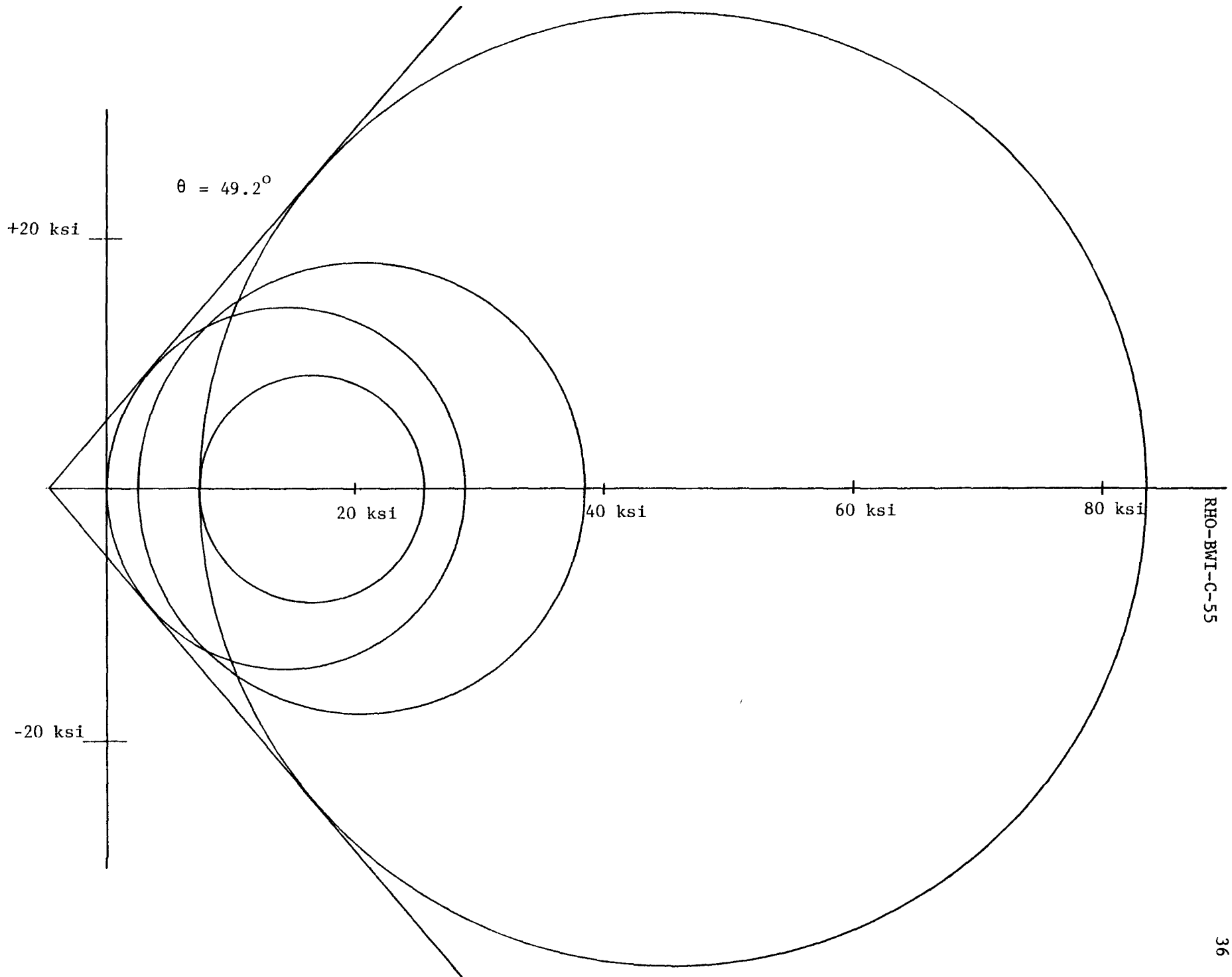


Figure 3.6: Mohr's Envelope - Triaxial Results 3660'-3690'



RHO-BMI-C-55

Figure 3.7: Mohr's Envelope - Triaxial Results 3730'-3750'

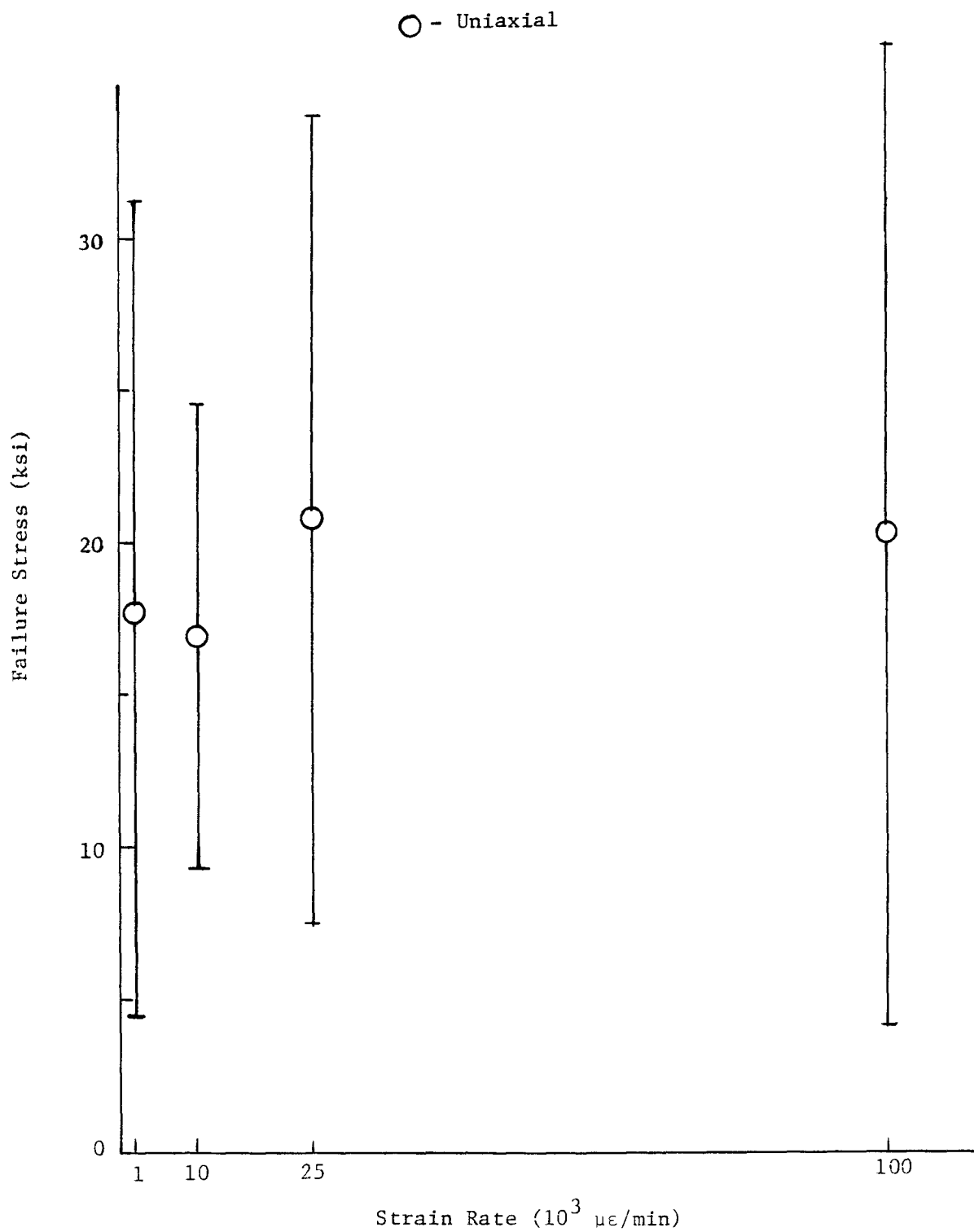


Figure 3.8: Failure Stress Versus Strain Rate

### 3.3 MEASUREMENT OF STRENGTH PROPERTIES OF JOINTED CORE UNDER VARYING AMBIENT CONDITIONS

#### 3.3.1 Apparatus

Joint testing was accomplished using the existing high-temperature triaxial cell, Terrametrics' hydraulic triaxial cells, and the MTS stiff testing machine.

#### 3.3.2 Test Specimens

Test specimens were right circular cylinders within tolerances specified in ASTM D-2938. The length was as close to 2 times the diameter as possible (except that shorter samples were used in these highly fractured sets of core). Exception is also taken to the ASTM D-2938 requirement for NX core (2-1/8 in. diameter), as most of the core was of smaller diameter (1-7/8 in.). The samples were oven dried overnight at 90°C, where required. The diameter and length were determined to within 0.01 in. and the weight measured to 0.1 gram. For the tests at high temperatures, the samples were heated overnight at the desired temperature prior to testing. Samples were chosen such that there was an apparent joint at a critical angle through the sample.

#### 3.3.3 Procedures

Compression tests on jointed samples were performed at varying ranges of temperature, confining pressure, and moisture content to determine their effect on strength and deformation properties of jointed basalt.

Tests were performed on 5 jointed samples, 2 of which were saturated prior to testing, at 4 temperatures (20, 150, 300, and 500°C), with each joint being tested sequentially at each temperature. Also, 5 jointed samples, 2 of which were saturated prior to testing, were tested at 4 confining pressures (1000, 2000, 3000, and 5000 psi). Each sample was loaded to failure for a given confining pressure. After the failure load had been determined, the

confining pressure was increased to the next level and the sample loading continued to the next failure.

The following properties were determined during the compression tests:

1. Compressive strength;
2. Cohesion;
3. Friction angle of joint surface.

Following testing, the joint infilling material was characterized in detail.

#### 3.3.4 Calculation

The compressive strength of the joint at each failure was calculated from:

$$\sigma_{ax} = \frac{F_f}{A} \quad (2)$$

where

$\sigma_{ax}$  = axial stress at failure (ksi);

$F_f$  = failure load (kips);

$A$  = sample cross-sectional area (in.<sup>2</sup>).

The friction angle of the joint surface was calculated for each slip after the first from:

$$\tan^{-1} \phi = \frac{\tau_n}{\sigma_n} \quad (3)$$

with

$$\tau_n = \text{joint shearing stress} = (\sigma_{ax} - \sigma_c) \sin \theta \cos \theta ; \quad (4)$$

$$\sigma_n = \text{joint normal stress} = \sigma_{ax} \sin^2 \theta + \sigma_c \cos^2 \theta ; \quad (5)$$

where

$\phi$  = friction angle of joint;

$\sigma_{ax}$  = axial failure stress (psi);

$\sigma_c$  = confining pressure (psi);

$\theta$  = joint slip angle, measured from vertical.

The inherent cohesion of the joint is calculated from the first slip of the joint using the formula:

$$\tau_i = \tau_n - F \sigma_n \quad (6)$$

where

$\tau_i$  = inherent cohesive joint strength (psi);

$\tau_n$  = joint shearing stress (psi);

$\sigma_n$  = joint normal stress (psi);

$F = \tan^{-1} \phi$  = joint friction factor - extrapolated from last three slips with a parabolic curve fit.

### 3.3.5 Test Results

Table 3.4 presents the results of the room-temperature and heated triaxial joint tests.

### 3.3.6 Test Data Analysis

Slip factors for the unheated triaxial joint samples show good consistency and exhibit the classical decrease with successive slips as the joint surface becomes increasingly polished. Joint strength can be expected to vary widely from joint to joint and, as such, is difficult to apply analytically. Joint strengths were comparable to those obtained for Series B, but were still lower than obtained for



TABLE 3.4

## INHERENT JOINT STRENGTHS AND SLIP FACTORS FOR JOINTED SAMPLES

## UNHEATED TRIAXIAL JOINTS

<u>Depth (ft)</u>	<u>Sample Number</u>	<u>Density (gm/cc)</u>	<u>Apparent Slip Factors (<math>\Delta \tau_n/\sigma_n</math>)</u>				<u>Joint Strength (psi)</u>
			<u>1 ksi</u>	<u>2 ksi</u>	<u>3 ksi</u>	<u>5 ksi</u>	
3656.0	TJ58 saturated	2.52	1.337	sample failed completely			
3673.0	TJ67	2.69	1.080	1.046	1.012	Failed	177
3685.3	TJ75 saturated	2.65	1.076	0.947	0.776	0.560	74
3737.9	TJ78	2.81	1.583	1.494	1.347	1.140	989
3783.1	TJ93	2.77	1.012	1.020	0.995	0.945	1449

## HEATED TRIAXIAL JOINTS

<u>Depth (ft)</u>	<u>Sample Number</u>	<u>Density (gm/cc)</u>	<u>Apparent Slip Factors (<math>\Delta \tau_n/\sigma_n</math>)</u>				<u>Joint Strength (psi)</u>
			<u>20°C</u>	<u>150°C</u>	<u>300°C</u>	<u>500°C</u>	
3648.0	TJ56	2.59	0	0.262	0.794	0.722	99
3661.2	TJ62	2.67	1.263	0.950	0.794	0.794	0
3685.0	TJ74	2.74	1.767	0.169	0.169	0.175	0
3689.7	TJ76	2.79	1.152	1.133	1.122	1.121	222
3755.9	TJ85	2.8	0.981	0.984	0.979	0.966	46

Series A. The friction factors were comparable and could be used for analytical applications at this time.

For two of the heated triaxial joint tests, the apparent slip factors decreased dramatically after heating to 150°C, but remained steady for further heating. Because of the subsequent insensitivity to temperature and the lack of this behavior in the other samples, it is believed that the decrease was not temperature induced, but due to interface destruction which occurred on the first slip. Based on the three series of tests, temperature affects only minimally the sliding behavior of joints, but may significantly affect joint strength.

### 3.4 MEASUREMENT OF THE THERMAL PROPERTIES OF INTACT CORE UNDER VARYING AMBIENT CONDITIONS

#### 3.4.1 Thermal Conductivity/Specific Heat Procedures

##### 3.4.1.1 Apparatus

The thermal properties tester is enclosed by a 10 in. diameter by 18 in. high-vacuum bell jar in a wire cage, and sealed and supported at the bottom by a massive aluminum base with feed-throughs for vacuum, hydraulic pressure, thermocouple wires, and electrical power. Inside the tester is a loading frame enclosing the instrumented test stack. The frame consists of 1-1/2 in. thick square steel plates on top and bottom, held together by four 1-in. diameter stainless steel threaded rods. Inside the loading frame, from top to bottom are: a stainless steel flatjack rated at 5000 psi at 600°C; a 1-in. thick ceramic insulating platen; a conical heater on a stainless steel form, providing a 5:1 area reduction from the flatjack to the sample (and a corresponding 5:1 increase in pressure); the sample test stack, consisting of 2 pyrex reference discs of well-known thermal properties the same size and shape as the sample; bracketing the sample, with 5 thermocouples in very thin aluminum discs (1 at each disc interface and 1 drilled into the sample); and, finally, a second conical heater identical to the top, but containing an integral spherical seat to ensure uniform loading.

The data are recorded on a strip chart (time base) recorder as the outputs of the 5 thermocouples and hydraulic pressure to the flatjack (from an internal pressure transducer) versus time. These data are multiplexed on the single pen recorder via an Omega Engineering "Dataplex 10" signal scanner.

The heating rates are controlled by Weathermeasure temperature controllers with controlling thermocouples placed in series opposed to a millivolt ramp generator.

#### 3.4.1.2 Test Specimens

Test specimens were 5/8-in. thick sections of core (right circular cylinders) approximately 2 in. in diameter. The faces were ground flat and parallel to within 0.0001 in.

#### 3.4.1.3 Procedures

Before each test, the spherical seat was tested for freedom of motion and lubricated with molybdenum grease, if deemed necessary. The bolts on top of the loading frame were loosened and the sample was inserted into its correct position. The thermocouples were checked for correct placement and the bolts atop the frame were tightened to secure the stack. Radiant heat shields of polished steel were placed around the test stack, the bell jar was positioned, and the system pressure was reduced.

At this point, the test was initiated. The flatjack was pressurized via a hand pump to 1/5 the desired stress on the sample. Then, the temperature controller inputs were balanced, the ramp generator was started, and heating begun. The test stack was heated from both ends simultaneously at a rate of about 3°C per minute. Previous experiments have shown this heating rate yields the most consistent results. The dataplex unit scans the hydraulic pressure and 5 thermocouples sequentially, and prints them as dashed lines on the strip chart recorder. Heating continued at a constant rate until the desired sample temperature was reached, at which time the ramp generator, heaters, and chart recorder were de-energized, air was admitted, and the test was concluded.

#### 3.4.1.4 Calculation

The system was designed to minimize convective and radiant heat transfer from the test stack by operating in a vacuum ( $10^{-4}$  mm. mercury pressure) and by surrounding the stack with a highly reflective radiant heat

shield. Thus, the system was idealized as a transient, one-dimensional conduction system with varying thermal properties.

This system was also used at Colorado State University in a similar setup. They were able to reduce Carslaw and Jaeger's equations to the simple set of formulae used in our calculations.

$$\alpha = \frac{L^2 v}{4 (T_2 + T_4) - 8T_3} \quad (7)$$

$$C_p = \frac{K'}{\rho L V} \frac{T_1 - T_2 + T_5 - T_4}{L'} - .965 \frac{V' L'}{\alpha'} \quad (8)$$

$$K = \rho C_p \alpha \quad (9)$$

where

$\alpha$  = thermal diffusivity of sample ( $\text{cm}^2/\text{sec}$ );

$C_p$  = specific heat of sample ( $\text{cal/gm } ^\circ\text{K}$ )

$K$  = thermal conductivity of sample ( $\text{watt/cm } ^\circ\text{K}$ );

$T_1$  = temperature at lower reference-heater interface ( $^\circ\text{K}$ );

$T_2$  = temperature at lower reference-sample interface ( $^\circ\text{K}$ );

$T_3$  = temperature at upper reference-sample interface ( $^\circ\text{K}$ );

$T_4$  = temperature at upper reference-heater interface ( $^\circ\text{K}$ );

$T_5$  = temperature at center of sample ( $^\circ\text{K}$ );

$L$  = thickness of sample ( $\text{cm}$ );

$V$  = heating rate of sample ( $= T_5$ ) ( $^\circ\text{K/sec}$ );

$\rho$  = density of sample ( $\text{gm/cc}$ );

$K'$  = thermal conductivity of pyrex references (watt/cm  $^{\circ}\text{K}$ );

$L'$  = thickness of pyrex references (cm);

$\alpha'$  = thermal diffusivity of pyrex references ( $\text{cm}^2/\text{sec}$ );

$V'$  = heating rate of pyrex references;  $(= \frac{\dot{T}_1 + \dot{T}_2 + \dot{T}_3 + \dot{T}_4}{4}) (^{\circ}\text{K}/\text{sec})$ .

### 3.4.2 Thermal Expansion

#### 3.4.2.1 Apparatus

The equipment used for the thermal expansion determinations consisted of a high-temperature dilatometer designed to use a vacuum and capable of continuously monitoring sample deformation with temperature. The unit is fully compensated for device-related deformations and has a programmable temperature control feature.

#### 3.4.2.2 Test Specimens

Test specimens were 1/4 in. in diameter and had a length of approximately 1.2 in. The ends were ground flat and parallel to within 0.001 in. The length was determined to within 0.001 in.

#### 3.4.2.3 Procedures

Prior to each series of tests, a specimen with a known coefficient of expansion was inserted in the dilatometer and heated over the test range to check unit operation. Then the sample of basalt was placed in the device, making sure contacts were clean and that the quartz probe moved freely. The thermocouples were then brought in contact with the specimen and the vacuum capsule slid over the holder and probe. The vacuum pump was energized and heating initiated. Sample temperature and thermal expansion were continuously recorded over the range of  $20^{\circ}\text{C}$  to the desired upper temperature.

### 3.4.2.4 Calculation

The coefficient of thermal expansion was then calculated:

$$\alpha_T = \Delta_L / L / \Delta_T \quad (10)$$

where

$\alpha_T$  = coefficient of thermal expansion (in/in-°C);

$\Delta_T$  = change in temperature (°C);

$\Delta_L$  = change in length for temperature change,  $\Delta_T$  (in.);

L = length of sample (in.).

### 3.4.2.5 Test Results

The results obtained from the thermal expansion tests are presented as a function of depth in Table 3.5.

TABLE 3.5

#### THERMAL EXPANSION COEFFICIENTS

<u>Depth (ft)</u>	<u>Sample Number</u>	<u>Density (gm/cc)</u>	<u>Temp. Range (°C)</u>	<u>Expansion Coefficient (x 10<sup>-6</sup> in/in - °C)</u>
3695.5	T19	2.78	222-364	9.60
3726.5	T15	2.78	197-412	8.26
3757.9	DC4XP308	2.68	134-414	11.96
3757.9	DC4XP308 (saturated)	2.68	98-426	8.15
3765.5	T22	2.77	166-357 407-480	10.40
3795.5	T24	2.76	147-497	7.34

#### 3.4.2.6 Test Data Analysis

The thermal expansion results for Series C were comparable to those obtained for both Series A and Series B. Again, it was not possible to obtain a sample from the upper portions of the flow area due to fracturing problems.

Thermal expansion was fairly linear over the range tested, with the same slight perturbation in the curves at around 100°C as observed in previous tests. The larger deviations in linearity observed for some samples in Series A at approximately 400°C did not occur for any of the samples in Series C. An unexplained difference in expansion coefficient did appear between the saturated and dried states for sample DC4XP308. As for Series B, obtaining required expansion samples proved difficult due to the highly fractured nature of the core.



### 3.5 CREEP TESTS

#### 3.5.1 Apparatus

The apparatus used consisted of Soiltest CT-710 series compression testing machines and heater jackets for the high-temperature tests. Deformations were recorded by dial gages.

#### 3.5.2 Test Specimens

Test specimens were right circular cylinders within tolerances specified in ASTM D-2938. The length was as close to 2 times the diameter as possible (except that shorter samples were required in these highly fractured cores). Exception was also taken to the ASTM D-2938 requirement for NX core (2-1/8 in. diameter), as the core was smaller in diameter (1-7/8 in.). The samples were oven dried overnight at 90°C where required. The diameter and length were determined to within 0.01 in. and the weight measured to 0.1 gram. For the tests at high temperatures, the samples were heated overnight at the desired temperature prior to testing.

#### 3.5.3 Procedures

The sample, with heater jacket when required, was inserted into the compression tester and a steady-state thermal condition established at the desired temperature. The required constant load was then applied to the specimen. Initial deformation readings were then taken. Deformations were continuously monitored at least daily, and the load and temperature maintained until a steady-state creep rate was attained. Ambient room temperature was recorded at each displacement monitoring.

#### 3.5.4 Calculation

The creep rate was continuously calculated by dividing the increase in strain by the time over which it occurs.

### 3.6 ROCK HARDNESS

#### 3.6.1 Apparatus

Scleroscope hardness tester.

#### 3.6.2 Test Specimens

Spare sections of core and unbroken thermal samples were used for hardness tests. A polished surface was used for the tests.

#### 3.6.3 Procedures

Ten or more indentations were made using the scleroscope tester, and the results averaged to determine a rock hardness.

#### 3.6.4 Calculation

The scleroscope hardness number was read directly from the machine, on a scale of 0-100, with 100 being an average value for hardened steel.

#### 3.6.5 Test Results

A scleroscope rock hardness test was performed on ten samples of basalt from along the length of the supplied core. The results of those tests as a function of depth are provided in Table 3.6.

#### 3.6.6 Test Data Analysis

Of the three series of cores, Series C samples had the highest hardness coefficients. Hardnesses were also the most consistent over the total depth range of the provided core and had a fairly low intra-sample variability.

Scleroscope hardness is plotted versus depth of core in Figure 3.9. Somewhat lower values are evidence for the upper and lower portions of the flow, but the correlation with depth is not as pronounced as in the two earlier series of tests.

Because of the significantly higher average hardness and lower standard deviation, it would appear that Series C (drill hole DC-4) was in fact harder than either Series A (drill hole DC-6) or Series B (drill hole DC-8).

TABLE 3.6

## SCLEROSCOPE HARDNESS COEFFICIENTS

<u>Depth</u> <u>(ft)</u>	<u>Sample</u> <u>Number</u>	<u>Density</u> <u>(gm/cc)</u>	<u>Mean</u>	<u>Hardness</u>	
				<u>Std. Dev.</u>	
3660.95	C161	2.64	66.2	7.60	
3668.95	C164	2.77	63.1	8.73	
3674.4	C70	2.69	80.6	7.04	
3682.85	C73	2.78	78.4	10.28	
3754.75	C82	2.82	82.9	7.08	
3754.75	C182	2.82	77.5	9.30	
3755.65	C184	2.76	63.0	24.77	
3764.55	C91	2.80	88.4	5.28	
3769.5	C97	2.76	53.4	12.21	
3787.75	C98	2.76	75.6	4.03	

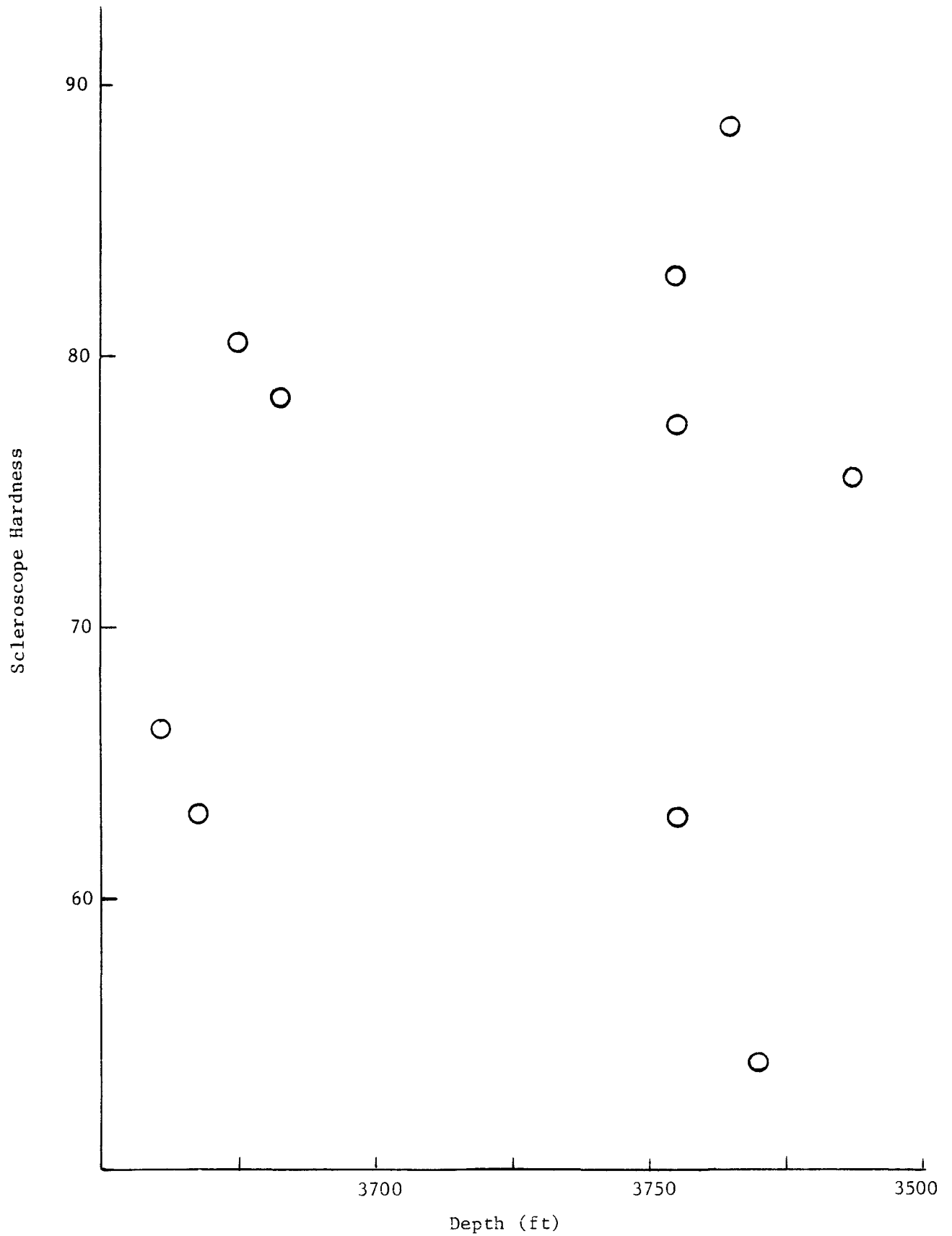


Figure 3.9: Scleroscope Hardness Versus Depth of Core

### 3.7 INVESTIGATION OF ANISOTROPY OF A SELECTED BASALT SAMPLE

#### 3.7.1 Apparatus

The equipment used for the dynamic wave velocities determinations consisted of:

1. 0.5 Megahertz (MHz) driver and pick-up longitudinal wave crystals manufactured by Panametrics;
2. 0.5 MHz driver and pick-up shear wave crystals manufactured by Panametrics;
3. Tektronix FG 502 function generator;
4. 2 Tektronix PG 501 pulse generators;
5. Tektronix AM 501 operational amplifier;
6. Tektronix DC 503 universal counter;
7. Tektronix 465 100 MHz dual trace oscilloscope;
8. 4-, 6-, 12-, and 18-in. aluminum calibration bars;
9. Ancillary leads and connectors.

#### 3.7.2 Test Specimens

The test specimens were the uniaxial and triaxial compression test specimens. Tolerances were well within those specified in ASTM D-2845.

#### 3.7.3 Procedures

Prior to each series of tests, the aluminum calibration bars were tested for both P and S wave velocity to determine if the equipment was working satisfactorily. Then the ends of the sample were carefully cleaned and a couplant jelly applied. The respective longitudinal or shear wave crystals were applied to the ends of the sample with uniform pressures and centered. A single cycle sine wave of the desired frequency (0.5 MHz for free medium P and S wave tests, 5 KHz for bar velocity determinations) was pulsed through the sample, and the travel time determined from the scope and counter.

Corrections for transducer and couplant thicknesses were determined from the tests on different length aluminum bars. The procedure was then repeated across the diameter of the specimen.

#### 3.7.4 Calculation

The compression and shear wave velocities were then calculated from:

$$V_p = L_p/T_p \quad (11)$$

$$V_s = L_s/T_s \quad (12)$$

where

$V_p$  = longitudinal wave velocity (m/s);

$V_s$  = shear wave velocity (m/s);

$L_p = L_s$  = length or diameter of specimen (m);

$T_p$  = travel time for longitudinal wave (sec);

$T_s$  = travel time for shear wave (sec).

#### 3.7.5 Test Results

Since an early modification of the contract eliminated the continuous monitoring of acoustic wave velocities, the only method available to find a sample displaying anisotropic acoustic behavior was to measure axial and radial P and S wave velocities on the compression samples. The results obtained from that survey are compiled in Table 3.7 by depth.

#### 3.7.6 Test Data Analysis

Shown in Table 3.7, along with recorded longitudinal and shear wave velocities, is the ratio of the respective wave velocities in the axial direction of the core to the velocity in the radial direction. Generally,

SERIES C

TABLE 3.7

DYNAMIC WAVE VELOCITIES AND RATIOS IN AXIAL AND RADIAL DIRECTIONS

<u>Depth (ft)</u>	<u>Sample No.</u>	<u>Vp ax (m/s)</u>	<u>Vp rad (m/s)</u>	<u>Vp ax/Vp rad</u>	<u>Vs ax</u>	<u>Vs rad</u>	<u>Vs ax/Vs rad</u>
3605.2	C51	4240	4181	1.01	2434	2610	0.93
3605.3	C151	4192	4334	0.97	2716	2540	1.07
3605.5	C52	3756	3606	1.04	2533	2461	1.03
3636.7	C53	4587	4415	1.04	2669	2846	0.94
3636.8	C153	4000	ND	ND	2424	2350	1.03
3645.7	C54	4560	4678	0.97	4350	2863	1.52
3645.8	C154	4826	4108	1.17	2738	2824	0.97
3647.7	C55	4572	4632	0.99	2707	2763	0.98
3647.8	C155	4648	4457	1.04	3734	2763	1.35
3650.0	C56	ND	ND	ND	ND	ND	ND
3655.7	C57	5011	4037	1.24	2767	2779	1.0
3655.8	C157	4966	ND	ND	2780	2916	0.95
3656.0	C58	ND	ND	ND	1530	2410	0.63
3656.3	C59	4833	4457	1.08	2963	2829	1.05
3656.4	C159	4924	2002	2.46	2790	3214	0.87
3657.6	C60	4790	4415	1.08	2825	2763	1.02
3657.7	C160	3702	4821	0.66	2824	3088	0.91
3660.9	C61	4279	4457	0.96	2734	2796	0.98
3661.0	C161	5050	5026	1.00	3096	3108	1.00
3661.2	C62	ND	ND	ND	2449	1071	2.29
3666.5	C63	5154	5192	0.99	2982	3150	0.95
3666.6	C163	5108	4415	1.16	3162	3214	0.98

RHO-BWT-C-55

SERIES C

Table 3.7 Continued

<u>Depth (ft)</u>	<u>Sample No.</u>	<u>Vp ax (m/s)</u>	<u>Vp rad (m/s)</u>	<u>Vp ax/Vp rad</u>	<u>Vs ax</u>	<u>Vs rad</u>	<u>Vs ax/Vs rad</u>
3668.9	C64	5017	5493	0.91	3251	3214	1.01
3672.4	C65	4938	5624	0.88	2856	3088	0.92
3672.7	C166	ND	2118	ND	1200	3008	0.39
3673.0	C67	ND	5460	ND	ND	2969	ND
3673.6	C68	2460	3042	0.81	2798	2894	0.97
3673.9	C169	5242	5163	1.02	3263	3369	0.97
3674.2	C70	5313	5365	0.99	3233	3271	0.99
3674.2	C170	ND	ND	ND	ND	ND	ND
3675.7	C71	ND	ND	ND	ND	ND	ND
3676.2	C72	ND	5624	ND	ND	3048	ND
3676.3	C172	ND	5523	ND	ND	3276	ND
3682.8	C73	5707	2386	2.39	3210	3399	0.94
3682.9	C173	5867	5208	1.13	5410	3338	1.62
3685.0	C74	ND	5937	ND	ND	3146	ND
3685.3	C75	ND	ND	ND	ND	ND	ND
3689.7	C76	ND	ND	ND	ND	3209	ND
3710.3	C77	4464	5576	0.80	3134	3416	0.92
3710.4	C177	7257	5976	1.21	5644	3364	1.68
3738.0	C78	ND	ND	ND	ND	ND	ND
3738.3	C179	5765	5394	1.07	3375	3158	1.07
3738.8	C80	3863	ND	ND	ND	ND	ND
3738.8	C180	ND	ND	ND	ND	ND	ND
3748.0	C81	ND	5715	ND	3170	3244	0.98
3748.1	C181	ND	6077	ND	3112	3357	0.93
3753.7	C184	ND	ND	ND	ND	ND	ND



SERIES C

Table 3.7 Continued

<u>Depth (ft)</u>	<u>Sample No.</u>	<u>Vp ax (m/s)</u>	<u>Vp rad (m/s)</u>	<u>Vp ax/Vp rad</u>	<u>Vs ax</u>	<u>Vs rad</u>	<u>Vs ax/Vs rad</u>
3754.7	C82	5877	5992	0.98	3800	3623	1.05
3755.0	C83	8063	6597	1.22	4536	3763	1.21
3755.1	C183	ND	ND	ND	ND	ND	ND
3756.2	C85	ND	ND	ND	ND	ND	ND
3756.5	C86	ND	ND	ND	ND	ND	ND
3756.9	C87	ND	6272	ND	ND	3820	ND
3756.9	C187	5707	5700	1.00	3669	3595	1.02
3757.3	C88	5806	5364	1.04	4516	3514	1.29
3757.4	C188	6258	5770	1.08	3510	3488	1.01
3765.1	C189	5025	5916	0.85	3179	3462	0.92
3769.5	C91	ND	5761	ND	2393	3375	0.71
3782.6	C92	ND	ND	ND	ND	ND	ND
3783.2	C93	ND	5026	ND	ND	3088	ND
3783.4	C94	4885	5192	0.94	3130	3088	1.01
3785.7	C95	ND	6057	ND	ND	3192	ND
3786.3	C196	2476	2339	1.06	3023	3068	0.99
3787.4	C97	ND	ND	ND	ND	ND	ND
3787.6	C198	ND	5692	ND	2669	3150	0.85

ND = Not determined

if this ratio deviates from 1.0 by over 10 percent, anisotropy is indicated. Very few of the samples tested showed anisotropy, indicating essentially isotropic elastic conditions within the basalt. Those samples which did indicate anisotropic behavior are being further characterized to determine the probable cause of the observed anisotropy.

As an indication of how the velocity varies with depth, the axial and radial P-wave velocities were plotted in Figure 3.10. A trend of increasing velocity with increasing depth is observable, but not to the degree found in the two other series of tests. The magnitude of the P-wave velocities was found to be higher in Series C than in Series B, but comparable to Series A. This further reinforces the differences observed in compressive strength and Young's modulus found among the three series of tests.

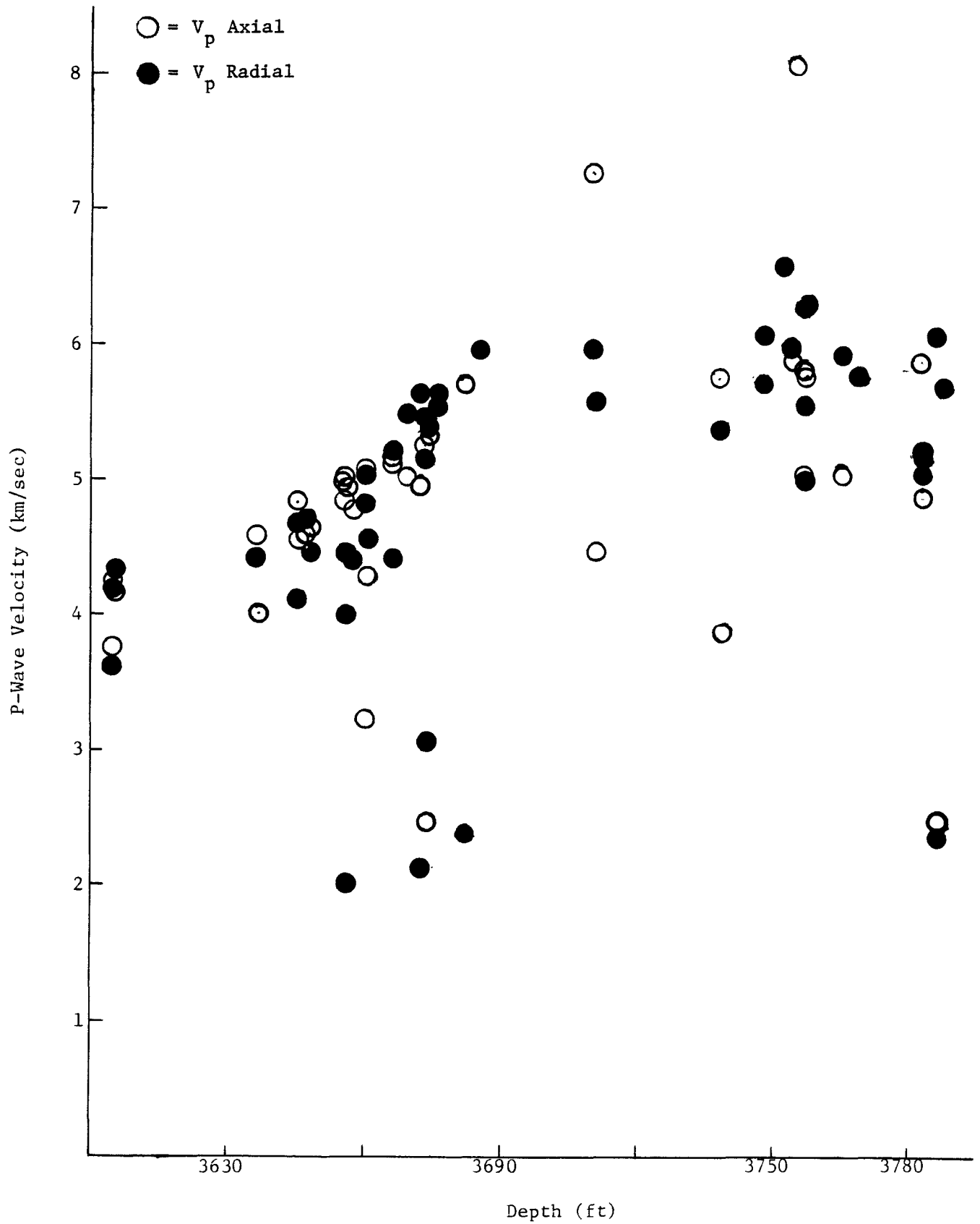


Figure 3.10: P-Wave Velocity Versus Depth

### 3.8 POST-FAILURE CHARACTERISTICS OF BASALT CORES

#### 3.8.1 Apparatus

The apparatus was the same as used for the uniaxial and triaxial testing, with the addition of steel stiffeners in parallel with the sample.

#### 3.8.2 Test Specimens

Test specimens were right circular cylinders within tolerances specified in ASTM D-2938. The length was as close to 2 times the diameter as possible (except that shorter samples were required in these highly fractured cores). Exception was also taken to the ASTM D-2938 requirement for NX core (2-1/8-in. diameter), as most of the core for this contract was smaller in diameter (1-7/8-in.). The samples were oven dried overnight at 90°C, where required. The diameter and length were determined to within 0.01 in. and the weight measured to 0.1 gram. For the tests at high temperatures, the samples were heated overnight at the desired temperature prior to testing.

#### 3.8.3 Procedures

Before each test, the calibration of the load cell and displacement transducers were checked. The stiffening frame was placed on the testing machine and the sample locked between the upper and lower plates. The stiffening frame was then loaded at a uniform rate which in turn loads the sample. The sample load was measured by a load cell in series with the sample inside the stiffener and displacements were measured by direct current displacement transducers. The complete load versus deformation curve was recorded, including the post-failure behavior, until the residual strength was reached.

#### 3.8.4 Calculation

The post-failure strength at any point was calculated by dividing the load at that point by the sample cross-sectional area.

### 3.8.5 Test Results

Three post-failure tests were performed, one at room temperature and pressure, one at high temperature and room pressure, and one at high pressure and room temperature. The first test at room temperature was the most successful, probably because it was from the top of the flow and was considerably less brittle than much of the core. The test at high pressure, as for Series A, was limited by machine capacity and the confining pressure had to be lowered to 1000 psi before failure could be induced. The first sample prepared for high-temperature testing essentially fell apart during preheating. The second high-temperature sample remained intact during heating, and a partially successful test was run.

Results obtained during the three tests are plotted in Figures 3.11, 3.12, and 3.13, respectively.

### 3.8.6 Test Data Analysis

Control of failure was better than in previous attempts on the other two series of cores, but a complete post-failure curve was not obtainable for any of the samples, thus confirming the brittle nature of basalt.

The sample at room temperature was weaker (from the upper portions of the flow) and showed a fairly uniform transition from elastic behavior to failure and into the post-failure region where a violent failure finally took place.

The high-confining pressure sample showed the expected high strength for a confined sample, with intermittent chipping as the failure load was approached. Violent failure also occurred for this sample shortly after entering the post-failure region.

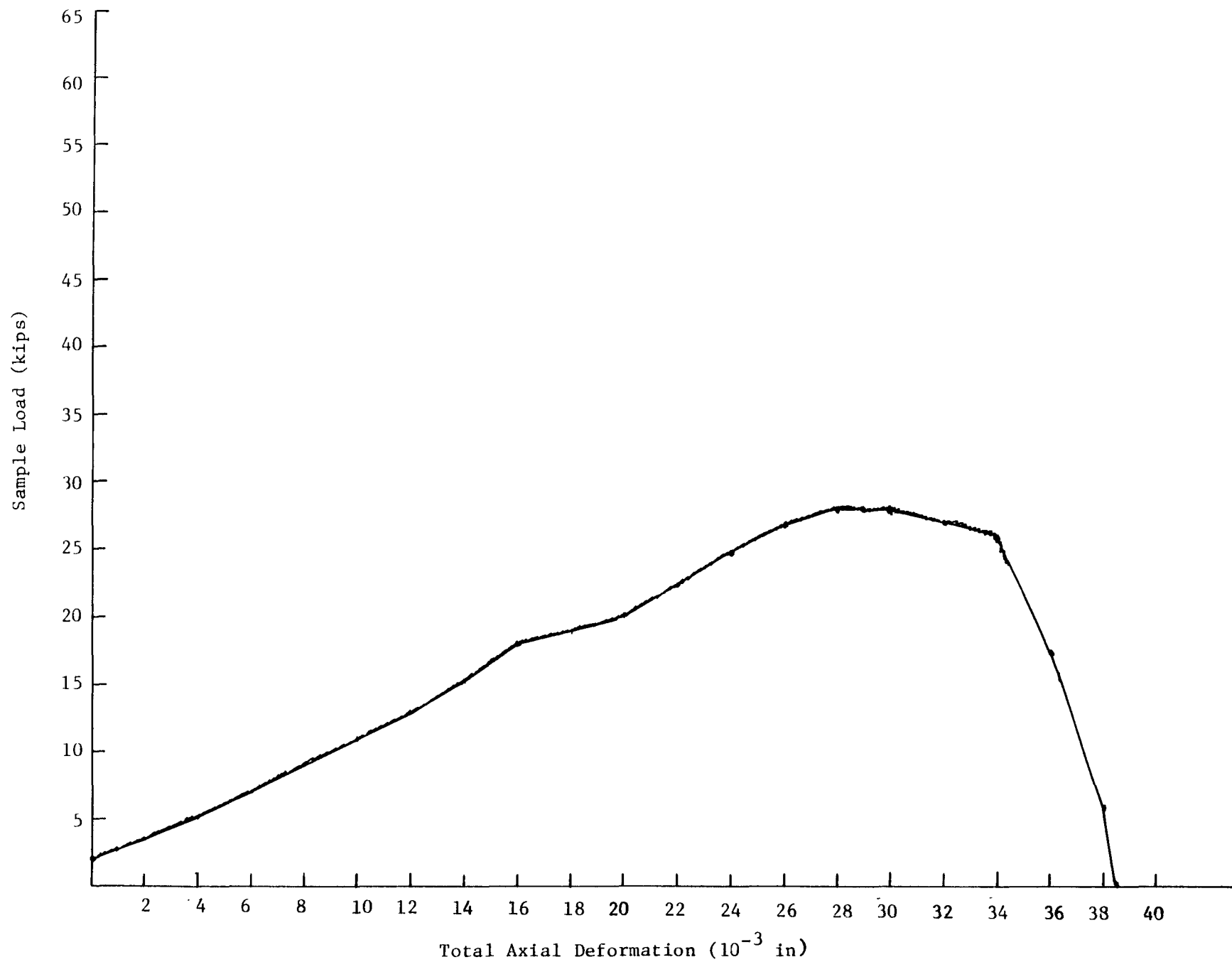
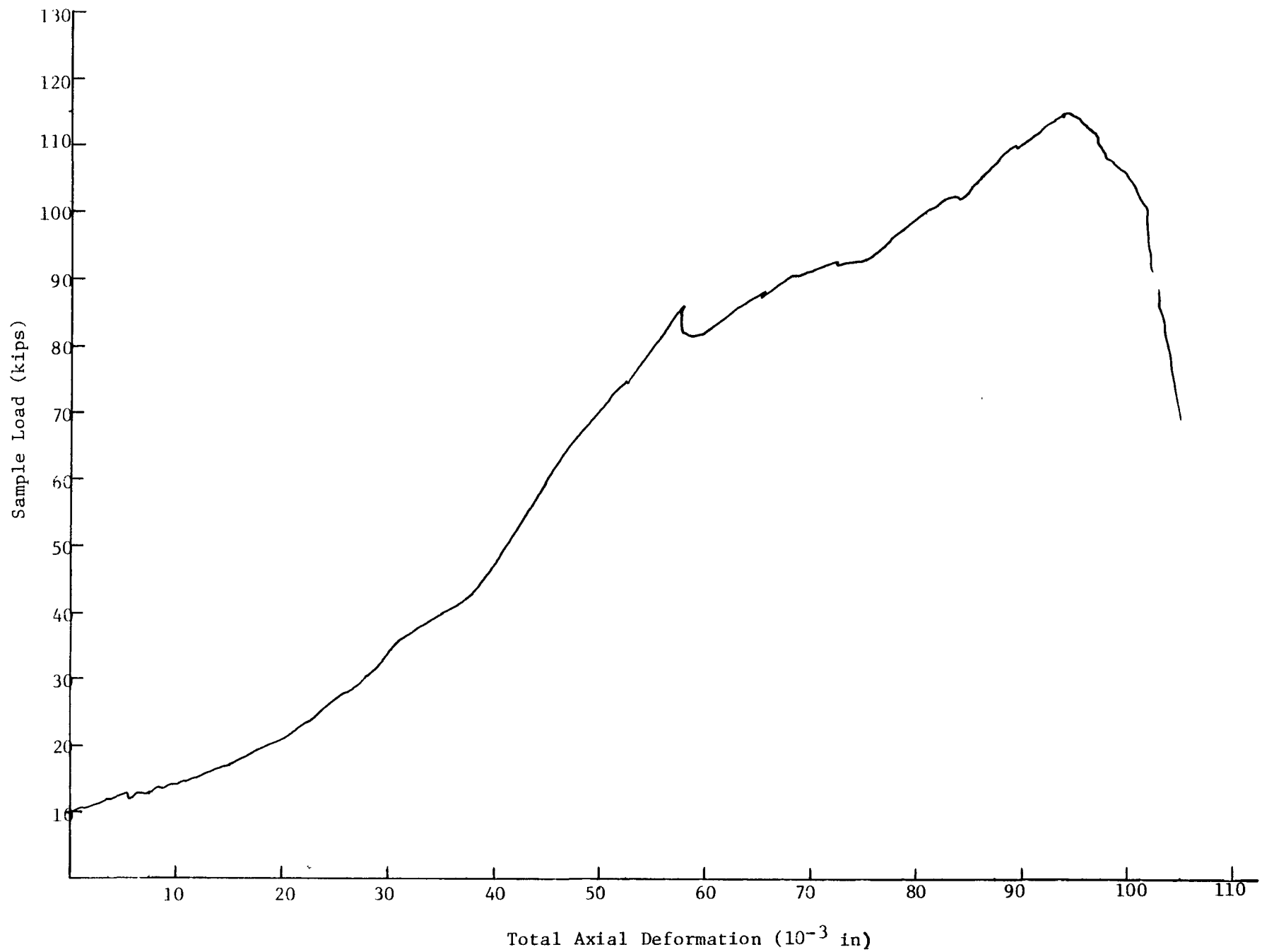


Figure 3.11: Room Temperature Post-Failure Test Graph



RHO-BWI-C-55

Figure 3.12: Triaxially Confined Post-Failure Test Graph

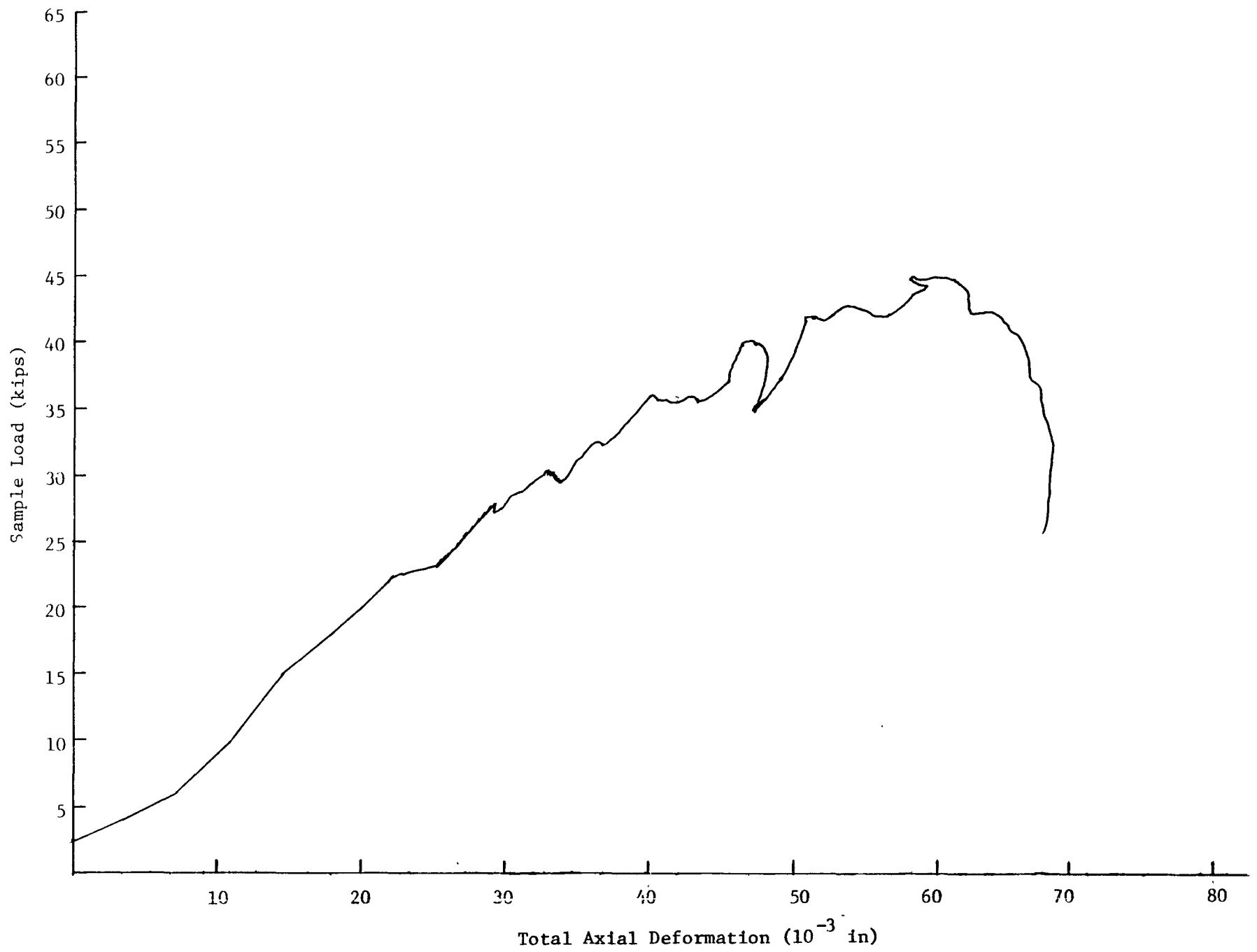


Figure 3.13: High-Temperature Post-Failure Test Graph



The high temperature post-failure test graph (Figure 3.13) is actually quite similar to the room-temperature and pressure results. There was some instability in the deformation measuring probes, since the probes were required to be mounted a safe distance away from the samples to prevent them being damaged by the heaters. The similarity between the room-temperature and high-temperature tests might indicate that the temperature used ( $500^{\circ}\text{C}$ ) had little or no effect on post-failure behavior.

It can be concluded that the basalt is a very brittle material, and difficult to control in the post-failure region.

### 3.9 PHYSICAL PROPERTIES

#### 3.9.1 Apparatus

The apparatus used for the density determinations consists of an analytical balance and precision micrometer calipers.

#### 3.9.2 Test Specimens

Test specimens were those used for the uniaxial and triaxial tests.

#### 3.9.3 Procedures

The prepared sample is dried for 24 hours at 105°C and weighed on a balance to within 0.1 gram. Length and diameter are measured to within 0.001 in.

#### 3.9.4 Calculation

The bulk density was determined as follows:

$$\rho_B = \frac{M_D}{\frac{\pi}{4} LD^2} \quad (13)$$

where

$\rho_B$  = bulk density (gm/cc);

$M_D$  = mass of dried sample (gm);

$L$  = sample length (cm);

$D$  = sample diameter (cm).

The apparent grain density can be determined by subtracting pore volume (determined from the porosity test) from the total volume of the sample.

#### 3.9.5 Test Results

The determined bulk density for each of the tested samples is provided in the results section under the appropriate tests. It should be noted that a

true density measurement was often quite difficult due to the fractured nature of the supplied core.

#### 3.9.6 Test Data Analysis

Bulk densities recorded were generally consistent for contiguous segments of core. Lowest densities were recorded for the upper portion of the flow, with densities increasing for the central portions of the flow. There is an indication of a slight drop in densities toward the bottom of the flow. Densities were quite similar between the three series of tests.

Density correlated well with many of the physical properties for the basalt and should be very useful as a preliminary gage of expected properties.

#### 4.0 GENERAL DISCUSSION

##### 4.1 COMPARISON TO PREVIOUS RESULTS

The results obtained from Series C samples were comparable to Series A and to FY 78 results. Strengths and modulus were quite similar to Series A, but differed significantly from Series B. Joint strengths were lower, yet friction factors remained consistent among the three series of tests. Thermal expansion remained similar to the Series A and Series B results, and remain higher than determined in FY 78. Anisotropy was less than determined for Series B and was very minor for Series A. Rock hardness was found to be higher than either Series A or Series B. Post-failure tests were more successful than in previous attempts, but still confirm the brittle nature of basalt. Densities and variations in densities were comparable. Variations in properties with density, and consequently the relative position in the flow, showed similar trends from the top of the flow to the bottom, with the exception that Series A evidenced a more pronounced reduction in densities near the bottom of the flow.

##### 4.2 LIMITATIONS OF SAMPLES, PROCEDURES, AND RESULTS

As for the previous series, the primary limitation to the current study is the reduced number of samples which were provided. It was necessary to obtain samples from every possible segment of core. Compressive sample lengths had to be reduced by half, waiving the ASTM requirement, and samples broken in coring, handling, or preparation had to be used (often patched with hydrostone or epoxied together from fragments) to perform the contracted number of tests. Thus, measured strengths may be higher than actual (in situ) strengths in many cases. The steps necessary to prepare the samples are noted on the data sheets.

The procedures are acceptable, given the qualitative nature of the study to date. When the site is chosen, a more detailed and thorough testing program should be undertaken to raise confidence levels in the generality and applicability of these data.

As discussed earlier, several factors limit the quantitative application of the data at this time. These include: the very limited amount of core supplied from which to select samples; the necessity of using reduced-size samples; the unavailability of mitigating physical features, such as chips, open joints, and voids within the samples; and the lack of sufficient replication for establishing confidence levels for various effects. Trends are now determinable for several parameters and statistical significances will be presented in a summary report.

## 5.0 CONCLUSIONS

The most significant conclusions to be made from the present set of tests are:

1. Series C (drill hole DC-4) uniaxial and triaxial compressive strengths were comparable to Series A (drill hole DC-6), but were significantly higher than Series B (drill hole DC-8);
2. Young's modulus also averaged approximately 50 percent higher than Series B, and was essentially the same as Series A;
3. Joint strengths were generally lower, but friction factors were quite similar to the previous series of tests;
4. There appeared to be a steady decrease in compressive strength with increasing temperature compared to little or no conclusive effect in Series A or Series B; also, the heated joints showed an average strength considerably below that of the unheated joints;
5. Confining pressure was found to significantly improve the compressive strength of basalt (the average strength of the confined samples was over twice that of the unconfined samples);
6. Thermal expansion coefficients were found to be similar to both Series A and Series B, but higher than determined during FY 78 testing;
7. Infrequent indications of anisotropy were observed for Series C;
8. Maintaining a controlled failure was again difficult due to the brittle nature of the basalt;
9. Density appears to be a good guide for relative physical properties, but not for absolute determinations, as evidenced by similar densities among the three series of tests, yet their differing physical properties.

RHO-BWI-C-55

Efforts are currently under way to further analyze trends within each series of tests and to analyze statistically the differences between the series; then, confidence intervals can be assigned to location and parametric effects. These findings will be presented in a summary report to follow.

6.0 DISTRIBUTIONNumber of  
Copies

3	<u>J. F. T. AGAPITO AND ASSOCIATES</u>
1	<u>AMOCO</u>  G. Servos
1	<u>ATOMICS INTERNATIONAL</u>  H. C. Wieseneck
6	<u>BATTELLE-OFFICE OF NUCLEAR WASTE ISOLATION</u>  N. E. Carter Library (5)
2	<u>BECHTEL INCORPORATED</u>  R. A. Langley, Jr.
1	<u>CALIFORNIA ENERGY RESOURCES CONSERVATION AND DEVELOPMENT COMMISSION</u>  E. Varanini
1	<u>CENTRAL WASHINGTON UNIVERSITY</u>  Department of Geology
6	<u>COLORADO SCHOOL OF MINES</u>  R. J. Miller (5) F. D. Wang
2	<u>DAMES &amp; MOORE</u>  G. Hocking T. Maini
1	<u>EASTERN WASHINGTON UNIVERSITY</u>  Department of Geology
1	<u>IDAHO BUREAU OF MINES AND GEOLOGY</u>  Library
1	<u>LAWRENCE BERKELEY LABORATORY</u>  J. A. Apps



Number of  
Copies

1	<u>LAWRENCE LIVERMORE LABORATORY</u>  L. D. Ramspott
2	<u>LOS ALAMOS SCIENTIFIC LABORATORY</u>  M. L. Wheeler K.     Wolfsberg
3	<u>NATIONAL ACADEMY OF SCIENCES</u>  W. E. Berg D.     Daley S.     Stuen
18	<u>NATIONAL ACADEMY OF SCIENCES - COMMITTEE ON RADIOACTIVE WASTE MANAGEMENT</u>  M.     Baram S. N. Davis E. L. Draper P. W. Durbin J. T. Edsall M.     Eisenbud J. A. Fay J. C. Frye E. F. Gloyna H. L. James R. E. Kasperson K. B. Krauskopf T. R. LaPorte C.     Mawson F. L. Parker T.     Pigford R.     Roy E.     Wenk, Jr.
1	<u>OREGON STATE DEPARTMENT OF GEOLOGY AND MINERAL INDUSTRIES</u>  J. D. Beaulieu
3	<u>PACIFIC NORTHWEST LABORATORY</u>  A. M. Platt R. W. Wallace Library
5	<u>SANDIA LABORATORIES</u>  E. H. Beckner R. C. Lincoln A. E. Stephenson L. D. Tyler W. D. Weart

Number of  
Copies

1	<u>STANFORD UNIVERSITY</u>
	I. Remson
1	<u>STATE OF IDAHO GOVERNOR'S OFFICE</u>
	C. Jones
1	<u>STATE OF OREGON GOVERNOR'S OFFICE</u>
	K. Woods
1	<u>STATE OF WASHINGTON GOVERNOR'S OFFICE</u>
	D. Jenkins
1	<u>SWEDISH NUCLEAR FUEL SUPPLY COMPANY (KBS)</u>
	L. B. Nillson
1	<u>U. S. BUREAU OF MINES</u>
	J. W. Corwine
2	<u>U. S. DEPARTMENT OF ENERGY-ALBUQUERQUE OPERATIONS OFFICE</u>
	D. T. Schueler
1	<u>U. S. DEPARTMENT OF ENERGY-COLUMBUS PROGRAM OFFICE</u>
	J. O. Neff
5	<u>U. S. DEPARTMENT OF ENERGY-HEADQUARTERS</u>
	C. R. Cooley
	M. W. Frei
	C. H. George
	C. A. Heath
	D. L. Vieth
1	<u>U. S. DEPARTMENT OF ENERGY-NEVADA OPERATIONS OFFICE</u>
	R. M. Nelson
2	<u>U. S. DEPARTMENT OF ENERGY-PUBLIC READING ROOMS</u>
	Richland, Washington
	Seattle, Washington

Number of  
Copies

6	<u>U. S. DEPARTMENT OF ENERGY-RICHLAND OPERATIONS OFFICE</u>  T. A. Bauman R. B. Goranson A. G. Lassila B. L. Nicoll D. J. Squires F. R. Standerfer
4	<u>U. S. GEOLOGICAL SURVEY</u>  G. D. DeBuchananne R. Schneider P. R. Steven W. S. Twenhofel
5	<u>U. S. NUCLEAR REGULATORY COMMISSION</u>  R. Boyle J. O. Bunting, Jr. J. C. Malaro J. B. Martin E. P. Regnier
1	<u>UNIVERSITY OF IDAHO</u>  Department of Geology
1	<u>UNIVERSITY OF MINNESOTA</u>  C. M. St. John
1	<u>UNIVERSITY OF OREGON</u>  Department of Geology
1	<u>UNIVERSITY OF WASHINGTON</u>  Department of Geology
1	<u>WASHINGTON PUBLIC POWER SUPPLY SYSTEM, INC.</u>  D. D. Tillson
2	<u>WASHINGTON STATE DEPARTMENT OF ECOLOGY</u>  P. M. Grimstad Library
2	<u>WASHINGTON STATE DEPARTMENT OF NATURAL RESOURCES</u>  V. E. Livingston Library

Number of  
Copies

1	<u>WASHINGTON STATE UNIVERSITY</u> Department of Geology
1	<u>A. C. WATERS</u>
1	<u>WESTERN WASHINGTON UNIVERSITY</u> Department of Geology
2	<u>WESTINGHOUSE WIPP PROJECT</u> R. C. Mairson
1	<u>WOODWARD-CLYDE CONSULTANTS</u>
31	<u>ROCKWELL HANFORD OPERATIONS</u> D. J. Cockeram T. A. Curran C. DeFigh-Price R. A. Deju H. B. Dietz R. G. Johnston M. R. Kasper, Jr. A. D. Krug J. G. Patricio E. S. Tepsa Basalt Waste Isolation Project Library (15) Document Control (4) Records Retention Center (2)